Review

Impact on transient stability of self-synchronisation control strategies in grid-forming power converters

Régulo E. Ávila-Martínez [a,b] [ID],*, Xavier Guillaud [c] [ID], Javier Renedo [b] [ID], Luis Rouco [a,b] [ID], Aurelio Garcia-Cerrada [a,b] [ID], Lukas Sigrist [a,b] [ID]

[a] *Instituto de Investigación Tecnológica (IIT), C. del Rey Francisco, 4, 28008, Madrid, Spain*
[b] *ETSI ICAI, Universidad Pontificia Comillas, Alberto Aguilera, 23, 28015, Madrid, Spain*
[c] *Laboratoire d'Electrotechnique et d'Electronique de Puissance (L2EP), Ecole Centrale de Lille, Cité Scientifique, CS 20048, Villeneuve d'Ascq, 59651, Hauts-de-France, France*

ARTICLE INFO

ABSTRACT

Grid-forming voltage source converters (GFM-VSCs) are emerging as a solution for integrating renewable energy resources (RERs) into power systems. GFM-VSCs need a self-synchronisation strategy to ensure that all converters and generators in the power system are in synchronism and they reach the same frequency in steady state. The self-synchronisation strategy in GFM-VSC that has received most attention in previous research is virtual synchronous machine (VSM) control. However, there has to date been no systematic study of the effects on transient stability of different variants of this strategy. This paper analyses and compares transient stability of four self-synchronisation strategies for GFM-VSCs: VSM without phase-locked loop (PLL), VSM with PLL, VSM without PLL using wash-out filter and integral-proportional (IP) controller. The paper also analyses two different methods that can be applied to GFM-VSC self-synchronisation strategies to improve transient stability: the concept of virtual unsaturated active-power controller (VAPC), proposed in previous work, and an algorithm for frequency limitation in the GFM-VSCs, which is proposed in this paper.

Contents

* Corresponding author at: ETSI ICAI, Universidad Pontificia Comillas, Alberto Aguilera, 23, 28015, Madrid, Spain.
E-mail addresses: regulo.avila@iit.comillas.edu (R.E. Ávila-Martínez), xavier.guillaud@cen-tralelille.fr (X. Guillaud), javier.renedo@ieee.org (J. Renedo), luis.rouco@iit.comillas.edu (L. Rouco), aurelio@iit.comillas.edu (A. Garcia-Cerrada), lukas.sigrist@iit.comillas.edu (L. Sigrist).

1. Introduction

Voltage source converters with grid-forming control (GFM-VSCs, for short) are emerging as the preferred solution for integrating renewable energy resources (RERs) into power systems [1–3]. GFM-VSCs require self-synchronisation control strategies, whose main philosophy is to mimic the behaviour of conventional synchronous machines. Self-synchronisation strategies are necessary to ensure that all GFM-VSC converters and synchronous generators in the system reach the same steady-state frequency [4]. Unlike for grid-following VSCs (GFL-VSC), a phase-locked loop (PLL) is not required for synchronisation in GFM-VSCs, and self-synchronisation strategies can be used instead.

Previous studies have proposed several variants of self-synchronisation strategies in GFM-VSCs, such as power synchronisation control [5], synchronverter control [6], virtual synchronous machine (VSM) control [7–9], active-power/frequency (P-f) droop control [10], integral-proportional (IP) controller [11], reactive-power-based synchronisation [12], virtual oscillator control (VOC) [13], among others. In VOC-based strategies, GFM-VSCs emulate non-linear oscillators and there are several variants. For example, in the dispatchable virtual oscillator (dVOC) [14], ensures almost global asymptotic stability of power system with 100% of converter-based generation, while allowing active-power dispatch of GFM-VSCs. Alternatively, the so-called matching control [15] uses a virtual oscillator control, in which the frequency of the GFM-VSC is calculated using the DC voltage, matching the dynamics of a synchronous machine. Authors in [16] analysed some of those different self-synchronisation strategies and proposed a variant to improve the dynamic response of the GFM-VSC by using a lead/lag filter. The work in [17] used a GFM-VSC scheme based on droop P-f control with an additional phase feed-forward term to improve the damping of the closed-loop system. Ref. [18] analysed the performance of different GFM-VSC self-synchronisation algorithms taking into account the primary energy source of the GFM-VSC power converter, and the work proposes a novel control scheme taking this aspect into account (so-called resource-aware grid-forming (RA-GFM)), improving the performance of the system. A summary of GFM-VSC strategies (in this case applied to high voltage direct current systems based on voltage source converters (VSC-HVDC)) can be found in [19] and GFM-VSC control applied to VSC-HVDC systems has been analysed in [20].

VSM self-synchronisation control has attracted considerable attention in power systems research and several variants have been described, including: VSM without phase-locked loop (PLL) [7], VSM with PLL [8,9] and VSM without PLL using a wash-out filter [21]. The work in [7] proved analytically that the known P-f-droop and VSM-without-PLL self-synchronisation strategies are equivalent. Ref. [22] analysed frequency estimator methods (PLL and frequency-locked loop (FLL), and with the frequency estimation applied at different points) in VSM and P-f droop GFM-VSC strategies by means of small-signal stability analysis, concluding that VSM-PLL strategy, with the frequency

estimation applied at the AC connection point, presents the best results in terms of performance and robustness.

It is essential to fully understand and ensure power system stability of power systems with large amounts of power converters, including GFM-VSCs. Power system transient stability is defined as large-disturbance angle stability and it is the ability of the generators of the system to remain in synchronism and reach a new stable steady-state equilibrium point when subject to large disturbances [23]. Although this phenomenon was originally related to conventional synchronous machines, research publications during the past years have shown that loss-of-synchronism phenomenon is also present in GFM-VSCs [24–28]. Furthermore, the work in [29] analysed the impact of GFM-VSC and GFL-VSC power converters on angle stability under larger disturbances in large-scale power systems, concluding that the former present better behaviour in terms of transient stability.

Different publications have analysed the transient stability of power systems with GFM-VSCs using different self-synchronisation strategies. Several studies [24–27,30–35] used VSM without PLL control (or P-f droop control) while another [11] proposed the IP controller. The latter study also proved the equivalence between the IP controller and VSM-with-PLL scheme under small disturbances; however, the performance of the latter under large disturbances was not analysed. Ref. [36] compared the performance of VSM-without-PLL and VSM-with-PLL schemes in terms of small-signal stability, but transient-stability performance was not analysed. Furthermore, researchers in [32] proposed the Transient Damping Method (TDM), a supplementary active-power set point (containing a proportional gain and a wash-out filter) to improve transient stability. This study was performed in VSM without PLL control. Although the configuration when using the TDM is similar to self-synchronisation strategy VSM without PLL control + wash-out, it is not exactly the same. To the best of the authors' knowledge, previous publications have not analysed the transient stability phenomenon in power systems with GFM-VSCs using VSM without PLL and with washout as self-synchronisation strategy.

Although the transient-stability performance of several GFM-VSC self-synchronisation strategies has been studied separately, a comparison of each of them has not been carried out in previous work. Hence, a comprehensive understanding of the transient-stability behaviour and the advantages and disadvantages of each of these strategies has not yet been reached.

This paper addresses this gap by providing a comprehensive analysis and comparison of the transient-stability performance of different GFM-VSC self-synchronisation control strategies, including VSM control (without and with PLL), VSM control without PLL and with wash-out and the IP controller technique. It analyses the advantages, limitations and performance characteristics of each self-synchronisation control strategy under different operating conditions in terms of transient stability.

A recent work [37] proposed the concept of virtual active-power control (VAPC) to improve the transient-stability performance of GFM-VSCs using a variant self-synchronisation strategy similar to VSM without PLL control, but with an additional degree of freedom. Later

studies [38,39] applied the concept of VAPC to GFM-VSCs using IP-control. Furthermore, Ref. [40] analysed transient stability of GFM-VSCs when using VSM without PLL and VAPC, proving the effectiveness of VAPC concept when using different priorities of $d - q$-axis currents in the current saturation algorithm of the power converter. However, the concept of VAPC has not been applied to GFM-VSC strategies VSM – without PLL or VSM – with washout explicitly in previous publications. Hence, questions that arise are whether the concept of VAPC is effective when using different self-synchronisation strategies and the comparison of the effectiveness of VAPC concept when using different GFM-VSC strategies. This paper addresses this gap and analyses systematically the impact of VAPC to the transient-stability performance of the most extended GFM-VSC self-synchronisation strategies.

The loss-of-synchronism phenomenon in GFM-VSCs occurs due to significant variations of the angle of the modulated voltage of the GFM-VSC, producing, therefore, significant variation on its frequency. Some methods applied to self-synchronisation strategies in GFM-VSCs seek to prevent loss of synchronism, by limiting directly or indirectly the output frequency of the GFM-VSC. The work in [11] proposed increasing the virtual inertia of the converter during the fault to improve transient stability. The inertia increase is activated when the current injection of the GFM-VSC reaches its limit. Ref. [41] proposed an adaptive P-f droop-based control method, which leads to an indirect limitation of the GFM-VSC output frequency, preventing loss of synchronism. The additional adaptive P-f droop term is introduced when the frequency of the GFM-VSC goes outside pre-defined limits. Research studies in [42–44] proposed a scheme for active-power/frequency limitation in GFM-VSCs, which consisted in limiting the active-power injection of the converter by changing its output frequency and limiting it with a saturator, improving both transient stability and frequency stability. The active-power/frequency limitation process is triggered when the active-power injection of the GFM-VSC goes outside its limits. Although main application of the frequency-limitation method proposed in [42,43] is frequency stability and limiting the GFM-VSC active-power injection when subject to power imbalances, it also helps to improve transient stability. The works in [45,46] proposed a frequency freezing strategy in GFM-VSCs to improve transient stability. When the current injection of the GFM-VSC reaches its limit, the output frequency of the GFM-VSC is freezed to the pre-fault frequency, preventing loss of synchronism. Finally, the work in [47,48] proposed a frequency saturation method in GFM-VSCs: a saturator is added to the output frequency of the GFM-VSC, which is activated if the frequency goes outside pre-defined limits. The work in [48] includes the additional condition that the derivative of the frequency has the same sign than the frequency. The work in [48] proposes the frequency saturator to improve transient stability explicitly, while the work in [47] just focus the study in fault-ride-through (FRT) performance of the GFM-VSC, but the paper does not analyse loss-of-synchronism phenomenon. Ref. [48] proposes to tune the frequency limits of each GFM-VSC using data of the whole power system (e.g., virtual inertia of all the GFM-VSCs of the system), to improve transient stability.

While Refs. [11,41–43,45–48] clearly prove the potential of frequency-limitation methods in GFM-VSCs to improve transient stability, there is still room for further improvement. For example, Refs. [11,41] limit the output frequency of the GFM-VSC indirectly; further improvements in terms of transient stability could be achieved if the output frequency of the GFM-VSC were limited directly during the fault. The work in [45,46] limits the output frequency of the GFM-VSC directly but it freezes the value to the pre-fault frequency. It would be desirable to maintain the GFM-VSC self-synchronisation behaviour as much as possible during the fault. Hence, a frequency saturator (as in [42,43,47,48]) rather than a freezed frequency may be more practical. Regarding the activation of the frequency limiter, in Refs. [11,45,46] the frequency limitation process is activated when the current injection of the GFM-VSC reaches its limit. Naturally, this occurs when a fault close to the converter occurs. However, the current limit could also be reached due to changes in the operating conditions or other disturbances, where the frequency limitation process may not be desirable or needed. In [41,47,48], the frequency limitation process is activated when the output frequency of the GFM-VSC reaches pre-defined limits, which may not distinguish if the event is related to a transient-stability or a frequency-stability issue. For example, if there is a power imbalance in the system the frequency of the centre of inertia of the system, the bus frequencies and the frequencies of the GFM-VSCs will change, but this does not necessarily mean that there is a transient stability issue: the frequencies of all GFM-VSCs of the system may be in synchronism during the transient. In fact, frequency excursions in a relatively small power system could be large due to power imbalances, but a single GFM-VSC could loss synchronism caused by a nearby fault, and at this moment and the frequency increment of the GFM-VSC could be much smaller than admissible frequency limits of the power system and the frequency of the GFM-VSC will be different than the frequencies of other generators, during the transient. The same issue occurs with the proposal of [42,43], which is activated when the active power injection of the GFM-VSC goes outside its limits.

Motivated by these publications [11,41–43,45–48], this paper proposes an algorithm for internal frequency limitation in GFM-VSC self-synchronisation strategies to improve transient stability (FLC, for short). In fact, some of the ideas of each strategy proposed in previous work are combined in such way that the advantages some of the strategies are used together, while some new features are also proposed here. Details will be provided in Section 4.2. The frequency limiter proposed in this work (FLC) is applied directly and it is only activated during the fault, which is detected with an voltage-based hysteresis characteristic, ensuring an explicit limitation in the frequency imposed by the GFM-VSC. In addition, the frequency limits are calculated around the pre-fault frequency, to avoid potential issues due to pre-fault steady-state frequency deviations. Hence, the proposed frequency limiter has advantages from a practical point of view. Finally, the frequency-limitation methods proposed in [11,41–43,45–48] are analysed for particular GFM-VSC self-synchronisation schemes, while this work analyses the proposed frequency limiter for different GFM-VSC self-synchronisation strategies.

Along the lines described above, the scientific contributions of this paper can be summarised as follows:

- Comprehensive analysis and comparison of transient-stability performance of different GFM-VSC self-synchronisation control strategies: VSM control without and with PLL, VSM control without PLL using a wash-out filter and IP controller.
- Analysis of the impact of the concept of VAPC to transient-stability performance of the studied GFM-VSC self-synchronisation strategies.
- Proposal of a simple but effective algorithm for frequency limitation (FLC) in self-synchronisation strategies in GFM-VSCs to improve transient stability.
- Analysis the impact on transient stability of the wash-out-filter time constant in VSM- with washout GFM-VSC strategy.

The analysis is carried out by ElectroMagnetic Transient (EMT) simulation in Matlab + Simulink + SimPowerSystems, using detailed average-type EMT models of power converters, including their controllers and operating limits.

The rest of the paper is organised as follows. Section 2 describes modelling and control aspects of GFM-VSCs, following the approach used in this paper. Section 3 presents the GFM-VSC self-synchronisation strategies that will be analysed and compared in the paper. Section 4 describes two methods to improve transient stability of GFM-VSCs, the concept of VAPC and the frequency limiter (FLC) proposed in this paper. Section 5 presents a theoretical analysis of transient-stability performance of the GFM-VSC self-synchronisation strategies and the concepts of VAPC and FLC. The case study and simulation results are presented in Section 6, including time-domain simulation and calculation of critical clearing times (CCT). Section 7 presents the conclusions of the paper. Finally, data used in the paper can be found in Appendix.
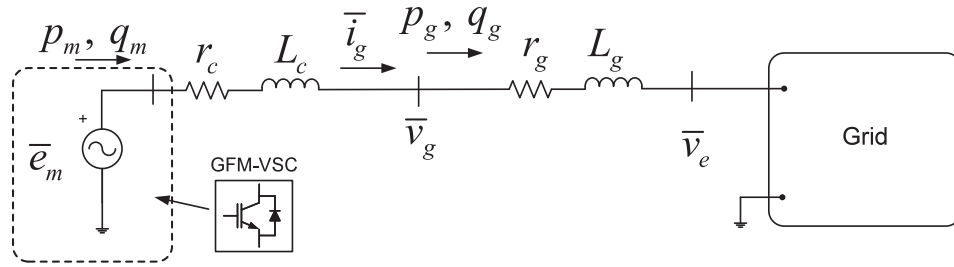
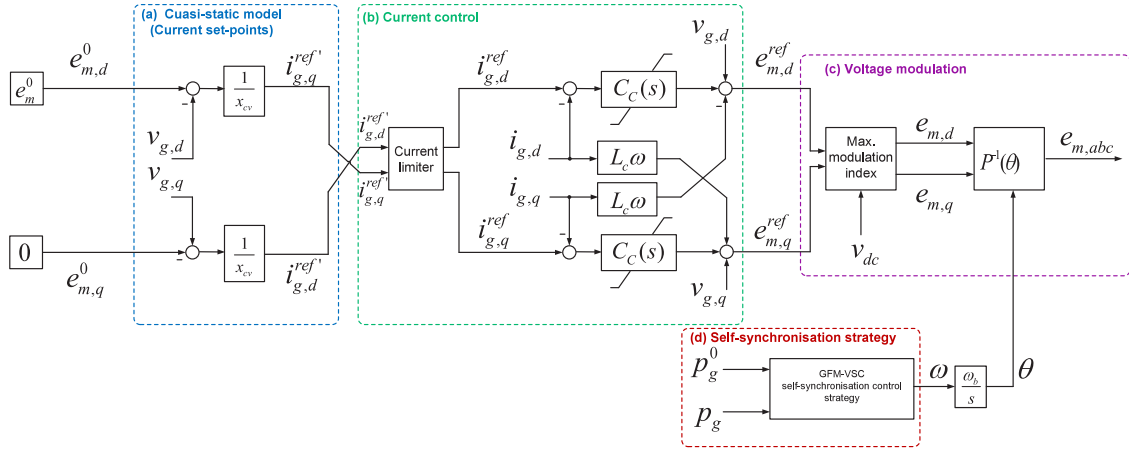**Fig. 1.** Equivalent model of a Grid-Forming Voltage Source Converter (GFM-VSC) connected to the grid.

Fig. 2. General scheme of the control system of a GFM-VSC.

2. Modelling and control of GFM-VSCs

Fig. 1 shows the scheme of a GFM-VSC connected to an infinite grid. $\bar{e}_m$ is the modulated voltage of the GFM-VSC, and $\bar{z}_c = r_c + jx_c$ ($x_c = L_c\omega$) is its series connection impedance, which includes its equivalent series reactor and the impedance of the connection transformer. The infinite grid has a voltage $\bar{v}_{e,i}$ and an equivalent impedance $\bar{z}_g = r_g + jx_g$. The voltage at Point of Common Coupling (PCC) of the GFM-VSC is $\bar{v}_g$ and the current and active- and reactive-power injections of the GFM-VSC at the PCC are $\bar{i}_g$, p_g and q_g, respectively.

Fig. 2 shows a general scheme of the control system of a GFM-VSC (see [38,49] for example). This work uses a current-controlled GFM-VSC approach. The GFM-VSC controller is based on vector control using a mobile $d - q$ reference frame, where the modulated voltage $\bar{e}_m$ is aligned with mobile $d - q$ axes: $e_{m,d} = e_m$ and $e_{m,q} = 0$. The GFM-VSC has a constant set point for the magnitude of the modulated voltage (e_m^0), and it uses a quasi-static model to calculate the current set points (marked with (a) in Fig. 2), following the approach of [21,38,49]:

$$i_{g,q}^{ref\,'} = \frac{v_{g,d} - e_{m,d}^0}{x_{cv}}, \quad i_{g,d}^{ref\,'} = \frac{e_{m,q}^0 - v_{g,q}}{x_{cv}}. \tag{1}$$

where $e_{m,d}^0 = e_m^0$ and $e_{m,q}^0 = 0$ and $x_{cv} = x_c + x_v$ is an equivalent virtual reactance used for current-setpoint calculation. The equivalent virtual reactance (x_{cv}) contains the true (or estimated) series reactance (x_c) and an additional virtual reactance (x_v). Notice that $x_v = 0$ pu could be used, or $x_v > 0$ pu if required to limit active-power variation in case of a phase shift.

A current controller is implemented ((b) in Fig. 2) with Proportional–Integral (PI) controllers and with a current limiter. Conventional Current Saturation Algorithm (CSA) is used for current limitation [30]. The outputs of the current controller are the $d - q$ set points of the modulated voltage, which are the inputs of the voltage modulation process of the GFM-VSC ((c) in Fig. 2).

Finally, the angle (θ) used for Park's transformation from $d - q$ components to three-phase signal is provided by the GFM-VSC self-synchronisation strategy ((d) in Fig. 2), which will be described in the next section. Notice that the frequency imposed by the modulated voltage of the GFM-VSC, ω, is the angular speed of the mobile $d - q$ reference frame used for vector control and it is determined by the self-synchronisation strategy.

3. Self- synchronisation control strategies of GFM-VSCs

Fig. 3 shows the general scheme of a self-synchronisation control, where the GFM-VSC imposes its frequency according to a specific control algorithm, ensuring synchronism with the rest of the system but maintaining its behaviour as a voltage source behind a series impedance. The active-power setpoint (p_g^0) is compared to the measured active-power injection (p_g) and the error is the input of the self-synchronisation strategy. The outputs are the frequency (ω, in pu) and angle (θ, in rad) of the modulated voltage of the GFM-VSC. The latter is used for Park's transformation (see Fig. 2). The angle δ is the angle of the modulated voltage with respect to a synchronous reference frame.

The objectives of GFM-VSC self-synchronisation strategies are as follows:

- To produce synchronising effect and ensure that the GFM-VSC reaches the same frequency than the rest of the system in steady state.
- When required, to produce an inertial response of the GFM-VSC.
- To control the dynamic response of the active- power injection of the GFM-VSC with sufficient damping, according to design specifications.

A primary frequency controller (or Primary Frequency Response, PFR) can also be included to the GFM-VSC. Nevertheless, this controller is considered as a different part and it is not included in the self-synchronisation strategy itself.
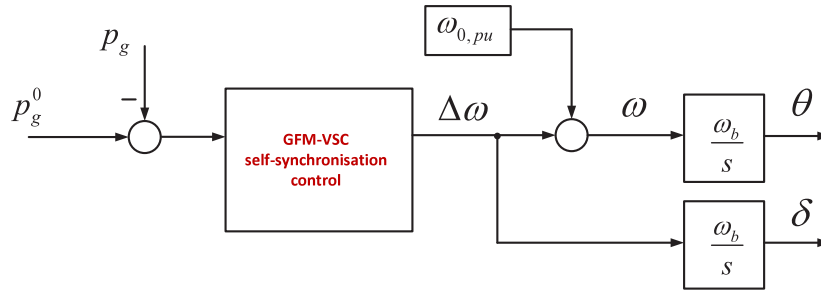
Fig. 3. General block diagram of a self-synchronisation control in GFM-VSCs.

Some of the most extended self-synchronisation strategies for GFM-VSCs will be analysed in this work, namely:

- **Strategy 1**: Virtual Synchronous Machine (VSM) without Phase-Locked Loop (PLL), hereinafter referred to as **VSM-noPLL** (see Fig. 4-(a)).
- **Strategy 2**: VSM with PLL, referred to as **VSM-PLL** (see Fig. 4-(b)).
- **Strategy 3**: VSM without PLL combined with a washout filter, referred to as **VSM-Washout** (see Fig. 4-(c)).
- **Strategy 4**: Integral Proportional (IP) controller, referred to as **IP control** (see Fig. 4-(d)).

Of the four self-synchronisation strategies, only strategy 1, VSM-noPLL (Fig. 4-(a)), which is equivalent to P-f droop control, has an implicit frequency control mechanism. This is because the inherent coupling between frequency dynamics and active power control allows the system to naturally respond to frequency deviations without the need for an additional control loop. In contrast, strategies 2, 3 and 4 (Fig. 4-(b)–(c)-(d)) decouple frequency and active power dynamics by incorporating a PLL (or another type of frequency estimator), a washout filter or a specific control structure, such as an IP controller. As a result, an external frequency control loop may be required to ensure adequate frequency regulation. Therefore, an explicit frequency control loop consisting of a proportional gain (K_{PFR}), a low-pass filter with a time constant (T_{PFR}) and a saturation limit (Δp_g^{max}) is implemented in these cases. In Fig. 4, ω_b is the nominal frequency in rad/s.

The details of each GFM-VSC self-synchronisation strategy are provided in next subsections.

3.1. Strategy 1: VSM-noPLL

Fig. 4-(a) shows the block diagram of the VSM without PLL. In this strategy, the GFM-VSC mimics the behaviour of a synchronous generator and it imposes its frequency according to the swing equation GFM-VSC [7,31].

The main characteristics of VSM-noPLL are as follows:

- The GFM-VSC provides an inertial response, due to the emulated inertia constant H_{GFM} (s).
- The damping factor coefficient, D_{GFM}, plays two roles simultaneously: (a) to provide damping and (b) to contribute to an instantaneous primary frequency response. Notice that it is mandatory that the primary frequency support is instantaneous, because, otherwise, the dynamic response of the GFM-VSC could be jeopardised. Notice also that if a typical value for the proportional gain of the frequency controller is used (e.g. $D_{GFM} = 20$ pu), then the dynamic response of the GFM-VSC is determined.

3.2. Strategy 2: VSM-PLL

Fig. 4-(b) shows the block diagram of the VSM with PLL, equipped with PFR control. In this strategy, the GFM-VSC imposes its frequency according to the swing equation, but using a PLL to estimate the frequency at the PCC [8,50]. Then, the difference between the frequency of the GFM-VSC and the estimated frequency of the grid at the PCC is multiplied by the damping coefficient D_{GFM}. The block diagram of the PLL equipped, which includes an anti-windup method, is shown in Fig. 5. Notice that, although this GFM-VSC self-synchronisation scheme uses a PLL, the application is totally different to the use of a PLL in grid-following converters. Here is only used to estimate the frequency of the grid and to be used in the self-synchronisation strategy.

The main characteristics of VSM-PLL are as follows

- The GFM-VSC needs an estimation of the frequency at the AC connection point, using a PLL.
- The GFM-VSC provides an inertial response, due to the emulated inertia constant H_{GFM} (s).
- The damping coefficient, D_{GFM}, is used to obtain the required damping ratio of the dynamic response of the GFM-VSC.
- The controller of the primary frequency response of the GFM-VSC is decoupled from the power control. For example, the PFR control can be made as slow as required (time constant T_{PFR}), without jeopardising the synchronising properties of the strategy. Notice also, that if primary frequency controller is not used (e.g. $K_{PFR} = 0$ pu), the GFM-VSC controls its active-power injection to a constant value (e.g. $p_g = p_g^0$).

3.3. Strategy 3: VSM-Washout

Fig. 4-(c) shows the scheme of the VSM without PLL, but incorporating a wash-out filter with a time constant T_{WD} [21,51]. This high-pass filter remains inactive during steady states but it acts during the transient.

The main characteristics of VSM-Washout are as follows:

- The GFM-VSC does not use a PLL.
- The GFM-VSC provides an inertial response, due to the emulated inertia constant H_{GFM} (s).
- The damping coefficient, D_{GFM}, is used to obtain the required damping ratio of the dynamic response of the GFM-VSC.
- The primary frequency controller of the GFM-VSC is decoupled from the power control, due to the washout filter.

3.4. Strategy 4: IP control

The IP controller is another approach for controlling GFM-VSC power converters described in [11]. This type of controller adds a proportional action (K_P) to the active power to provide damping, as shown in Fig. 4-(d).

The main characteristics of IP control are as follows:

- The GFM-VSC does not require an estimation of the frequency at the AC connection point.
- The GFM-VSC provides an inertial response, due to the emulated inertia constant H_{GFM} (s).
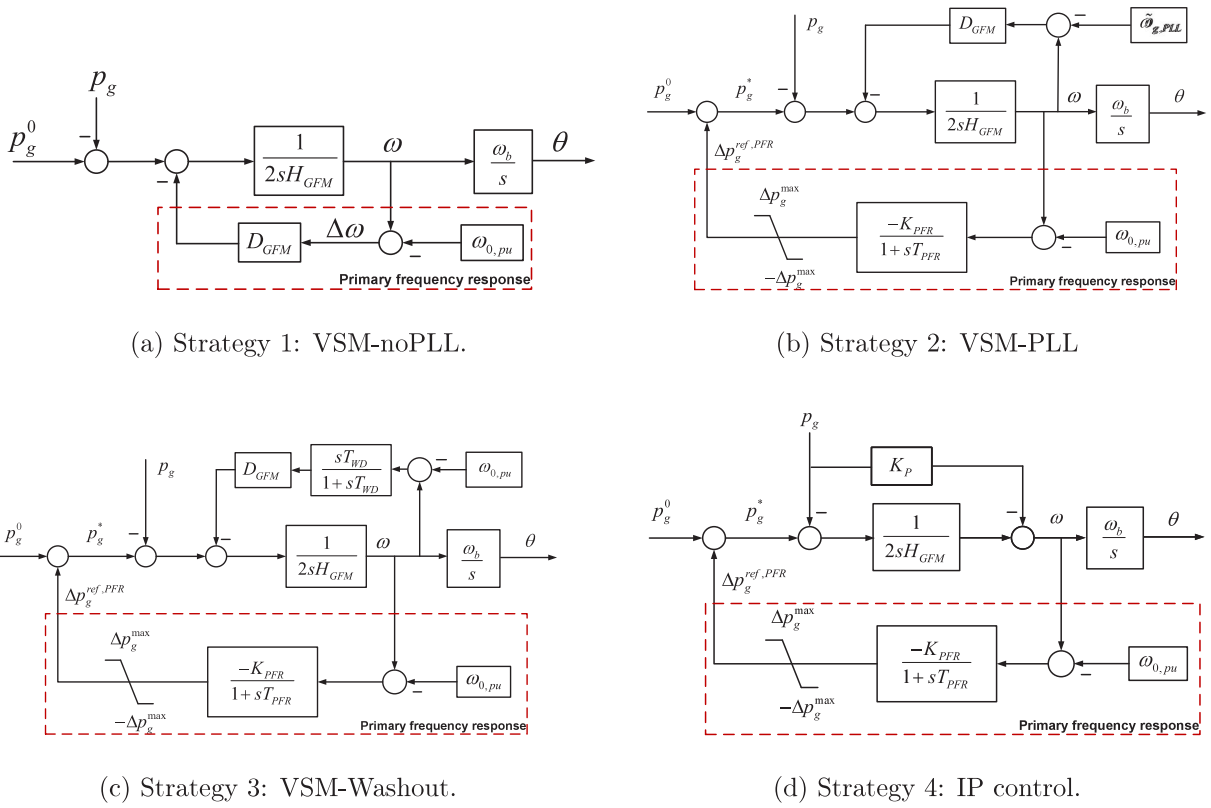
(a) Strategy 1: VSM-noPLL.

(b) Strategy 2: VSM-PLL

(c) Strategy 3: VSM-Washout.

(d) Strategy 4: IP control.

Fig. 4. Different self-synchronisation control strategies in GFM-VSCs with primary frequency response (PFR) control.
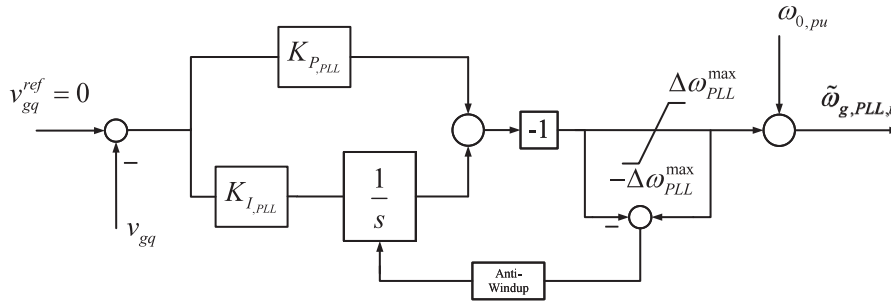

Fig. 5. PLL block diagram equipped with an anti-windup.

- The proportional gain, K_P, is used to obtain the required damping ratio of the dynamic response of the GFM-VSC.
- The primary frequency controller of the GFM-VSC is decoupled from the self-synchronisation control. Then an external control loop for PFR support can be added to the GFM-VSC control (Fig. 4-(d)).
- As will be explained in Section 3.5, the behaviour of IP controller under small disturbances is equivalent to the behaviour of VSM-PLL strategy [11].

3.5. Design of self-synchronisation strategies

Parameters of the GFM-VSC self-synchronisation strategy will be designed as follows:

- To obtain a dynamic response of the GFM-VSC with the required characteristics.
- When possible, the PFR controller is designed separately, using a typical values for the proportional gain.

The analysis is based on the one carried out in previous work [2,11] and the details are omitted in this paper.

The system of Fig. 1 is considered. Firstly, a GFM-VSC with VSM-PLL is considered. The PFR controller is assumed to be slow and it is neglected from the analysis. It can be shown that, under small disturbances, the transfer function between the active-power set point and output of the GFM-VSC ($T_{(s)} = p_g/p_g^*$) can be written as [2,11]:

$$T(s) = \frac{p_g(s)}{p_g^*(s)} = \frac{\left(\frac{\omega_b}{2H_{GFM}x_c}\right)}{s^2 + \frac{D_{GFM}}{2H_{GFM}}s + \frac{\omega_b}{2H_{GFM}x_c}} \quad (2)$$

Hence, the damping ratio, ζ, and the natural frequency, ω_n, are given by:

$$\zeta = \frac{D_{GFM}}{4H_{GFM}}\frac{1}{\omega_n}, \quad \omega_n = \sqrt{\frac{\omega_b}{2H_{GFM}x_c}}. \quad (3)$$

There are two Eqs. (3) and four parameters (H_{GFM}, D_{GFM}, ζ and ω_n).

In the case of VSM-noPLL strategy, under the assumption that the estimated frequency at the PCC is similar to the frequency of the infinite grid, which is an approximation assuming a strong grid, Eq. (3) also

Table 1
Design of GFM-VSC self-synchronisation strategies.

Strategy	Specified values	Calculated values
Strategy 1: VSM-noPLL	H_{GFM}, D_{GFM} PFR (implicit): $K_{PFR} = D_{GFM}$ $T_{PFR} = 0$ s	ζ and ω_n, with (3)
Strategy 2: VSM-PLL	H_{GFM}, ζ PFR: K_{PFR}, T_{PFR}	D_{GFM} and ω_n, with (3)
Strategy 3: VSM-Washout	H_{GFM}, ζ PFR: K_{PFR}, T_{PFR} Wash-out: T_{WD}	D_{GFM} and ω_n, with (3)
Strategy 4: IP control	H_{GFM}, ζ PFR: K_{PFR}, T_{PFR}	K_P and ω_n, with (4)

holds. In the case of VSM-Washout strategy, the same approximation is made plus the approximation that the wash-out filter has low effect and it is neglected. This is only true if the wash-out time constant (T_{WD}) is high enough. Then, Eq. (3) can also be used. Further considerations about the design aspects and the wash-out-filter time constant in VSM-Washout are described in Section 3.6.

The work in [11] proved the equivalence between VSM-PLL and IP control, with where $D_{GFM} = 2H_{GFM}K_P\omega_b/x_c$. Therefore, in IP control the damping ratio and natural frequency are related to the control parameters as follows [11]:

$$K_P = \zeta\sqrt{\frac{2x_c}{H_{GFM}\omega_b}} \quad \text{and} \quad \omega_n = \sqrt{\frac{\omega_b}{2H_{GFM}x_c}}. \tag{4}$$

Therefore, the design of GFM-VSC self-synchronisation strategies used in this work is as summarised in Table 1.

3.6. Design of self-synchronisation strategies - Specific aspects of strategy 3 (VSM-Washout)

As described previously, Strategy 3 (VSM-Washout), Eq. (3) and Table 1 could also be used for the design, taking into account small-signal stability aspects and using the assumption that the wash-out-filter (T_{WD}) is high enough. Nevertheless, in Strategy 3 (VSM-Washout), transient-stability behaviour should be also taken into account. In previous work, the design of the wash-out filter time constant in strategy VSM-Washout has not been addressed explicitly. However, Ref. [52] has analysed the impact of the wash-out filter in the so-called transient damping method (TDM), and conclusions can be applied directly to the VSM-Washout strategy. The work in [52] proposes a curve for feasible regions of parameters D_{GFM} and T_{WD}, in terms of transient stability. Mainly, in order to use high values of D_{GFM}, the wash-out filter time constant should be high enough, concluding that $T_{WD} \geq 1$ s could be a reasonable value, for the test system analysed. In addition, in Strategy 3 the wash-out filter adds a state variable and the closed-loop system dynamics is more complex and it is not a second-order system any more. However, this aspect can be addressed by using a high enough value of T_{WD} and it is recommended to check the results of the design by time-domain simulation. Obviously, the wash-out filter time constant T_{WD} should not be excessively high, because it would not be able to avoid active-power changes under frequency offsets, which is its role.

4. Methods to improve transient stability

This paper also analyses two methods to improve transient stability in GFM-VSCs, which could be applied to all GFM-VSC self-synchronisation strategies of Section 3:

- Virtual active power control (VAPC), proposed in previous work [37].
- A frequency limiter for GFM-VSC control (FLC), proposed in this paper.

4.1. Virtual active power control (VAPC)

The virtual active power control (VAPC) was proposed in [37] to improve transient stability in GFM-VSCs. In VAPC, the GFM-VSC uses as feedback signal of the self-synchronisation mechanism the *unsaturated virtual active power*, p_g^{virt}, instead of the measured active power injection, as shown in Fig. 6. Notice that VAPC is compatible with any self-synchronisation mechanism in GFM-VSCs.

The unsaturated virtual active power used in VAPC (p_g^{virt} in Fig. 6) is calculated as follows:

$$p_g^{virt} = v_{g,d} \cdot i_{g,d}^{ref'} + v_{g,q} \cdot i_{g,q}^{ref'} \tag{5}$$

where $v_{g,d}$ and $v_{g,q}$ are the voltage components at PCC and $i_{g,d}^{ref'}$ and $i_{g,q}^{ref'}$ are the unsaturated current set points.

All details and analysis of VAPC control can be found in [37].

4.2. Proposed frequency limiter control (FLC)

In this Section, a frequency limiter (FLC) in GFM-VSCs is proposed to improve transient stability. The proposed frequency limiter was motivated by previous work in [11,41–43,45–48], but it introduces new features to improve its performance, as discussed in Section 1. The proposed frequency limiter in GFM-VSCs: (a) aimed to improve transient stability, (b) it is activated during when a fault is detected, by looking to the terminal voltage and using a hysteresis characteristic, and (c) it includes a frequency saturator around the pre-fault steady-state frequency.

Fig. 7 shows the block diagram of the proposed algorithm for frequency limitation in GFM-VSCs to improve transient stability. The proposed frequency limiter consists of the following elements:

- Fault Detection: It is performed with a hysteresis characteristic:

  – A binary variable γ_1 is used, which is set to 1 upon detection of a voltage decrease with a hysteresis, as illustrated in Fig. 7.
  – If $v_g \leq v_A$ (fault detected), then $\gamma_1 = 1$ and remains at 1 until $v_g > v_B$. If a fault is not detected, $\gamma_1 = 0$.

- Frequency Saturator: It is activated only when the fault is detected, limiting the frequency if it exceeds a specific threshold: ω^{max}, ω^{min}.
- Anti-Windup mechanism: When the frequency saturates, it resets the integral part of the self-synchronisation mechanism (i.e., the integral of the virtual inertia).

The frequency limits of the proposed frequency-limitation algorithm is given by:

$$\begin{aligned} \omega^{max} &= \omega^{steady-state} + \Delta\omega^{max} \\ \omega^{min} &= \omega^{steady-state} - \Delta\omega^{max} \end{aligned} \tag{6}$$

where:

- ω^{max} is the maximum saturated frequency.
- ω^{min} is the minimum saturated frequency.
- $\omega^{steady-state}$ is the unsaturated frequency of the converter in steady-state before the fault. Notice that the steady-state pre-fault frequency is used here, to avoid dependency on steady-state frequency deviations in the system.
- $\Delta\omega^{max}$ is the maximum increment of the frequency of the GFM-VSC. This parameter should be designed (e.g. $\Delta\omega^{max} = 0.005$ pu, for example).
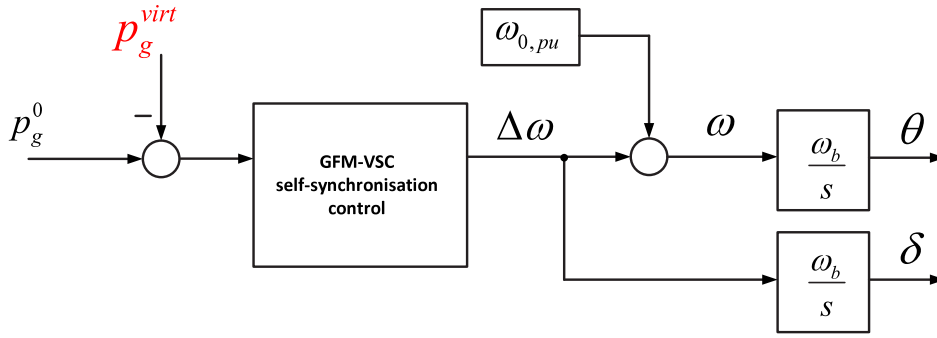
Fig. 6. General block diagram of a self-synchronisation control in GFM-VSCs using the virtual active power p_g^{virt} as a feedback measurement.
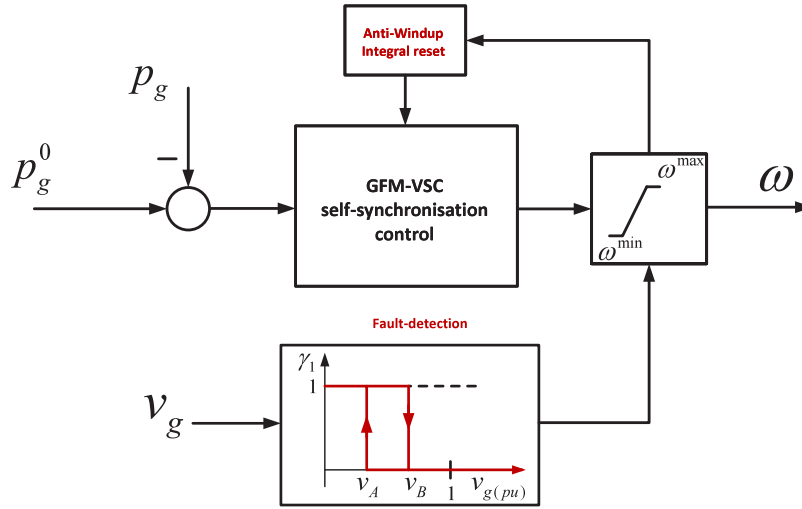

Fig. 7. Proposed frequency limiter applied in GFM-VSC self-synchronisation strategies.

5. Theoretical analysis

This section presents a theoretical analysis on the impact on transient stability of self-synchronisation strategies in GFM-VSCs, the concept of virtual active power control (VAPC) and the proposed frequency limiter for GFM-VSCs. Active power–angle ($P - \delta$) curves are used for the analysis, following the guidelines used in previous work [28,30,32, 33,35,37,53]. In synchronous machines, Equal Area Criterion (EAC) is used for the theoretical transient stability analysis [54,55]. However, although the EAC could provide some qualitative insight of transient-stability behaviour of GFM-VSC power converters, it cannot be applied directly to GFM-VSCs, as shown in [56]. This is mainly due to the fact that the high damping coefficient used in GFM-VSCs is much higher than the one in synchronous machines. This implies that, after the fault clearing, the angle of the GFM-VSC increases much less than the rotor angle in synchronous machines, as illustrated in [3].

Hence, the key aspects taken into account for the theoretical analysis are as follows:

- $P - \delta$ curves: The larger is the $P - \delta$ curves, the larger is transient-stability margin of the GFM-VSC and this will result in a higher critical clearing time (CCT) of the fault, as shown in previous work [28,30,32,33,35,37,53].
- Structure and differential equation of the GFM-VSC self-synchronisation strategy and methods to improve transient stability: if a fault occurs, the best results in terms of transient stability are obtained with strategies in which the frequency and angle increase less, during the fault and after the fault clearing. This depends on each strategy.

A GFM-VSC is connected to an infinite grid, as shown in Fig. 8. It is assumed that the external grid is strong (x_g low) and the series resistances are neglected, for illustrative purposes. The control system of the GFM-VSC is as the one described in Fig. 2 of Section 2, where the virtual impedance of the quasi-static model is assumed to be zero ($x_v = 0$), hence $x_{cv} = x_c$. A conventional Current Saturation Algorithm (CSA) is used for current limitation of the GFM-VSC, with equal priority to d- and q-axis current injections. The magnitude of modulated voltage of the GFM-VSC is assumed to be constant for the analysis ($e_m = e_m^0$).

The active power injection of the GFM-VSC, when the current limit has not been reached, reads:

$$p_g = p_e = \frac{e_m v_e}{x_{tot}} \sin \delta \tag{7}$$

where δ is the angle of the modulated voltage of the GFM-VSC (with respect to the external grid) and $x_{tot} = x_c + x_g$.

A three-phase-to-ground short circuit is applied at bus e at a certain time t_f (for illustrative purposes) and it is cleared at a certain time t_{cl}. When the fault is cleared, the angle of the modulated voltage of the GFM-VSC is called δ_{cl}. When the fault occurs, $v_e = 0$ and, therefore, the active-power injection of the GFM-VSC goes to zero too: $p_g = 0$.

When the GFM-VSC has current limiter CL-CSA, the active-power injection of the GFM-VSC is given by [37,38]:

$$p_g = \begin{cases} \dfrac{e_m^0 v_e}{x_{tot}} \sin \delta, & \text{if} \quad \delta < \delta_a \ (i_g < i_g^{\max}) \\ \dfrac{e_m^0 v_e \sin \delta}{\sqrt{(e_m^0)^2 + v_e^2 - 2 e_m^0 v_e \cos \delta}} \cdot i_g^{\max}, & \text{if} \quad \delta \geq \delta_a \ (i_g = i_g^{\max}) \end{cases} \tag{8}$$

where δ_a is the angle at which the current injection of the GFM-VSC reaches its current limit ($i_g = i_g^{\max}$).
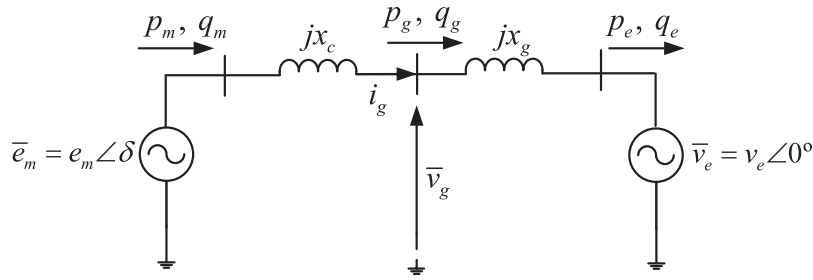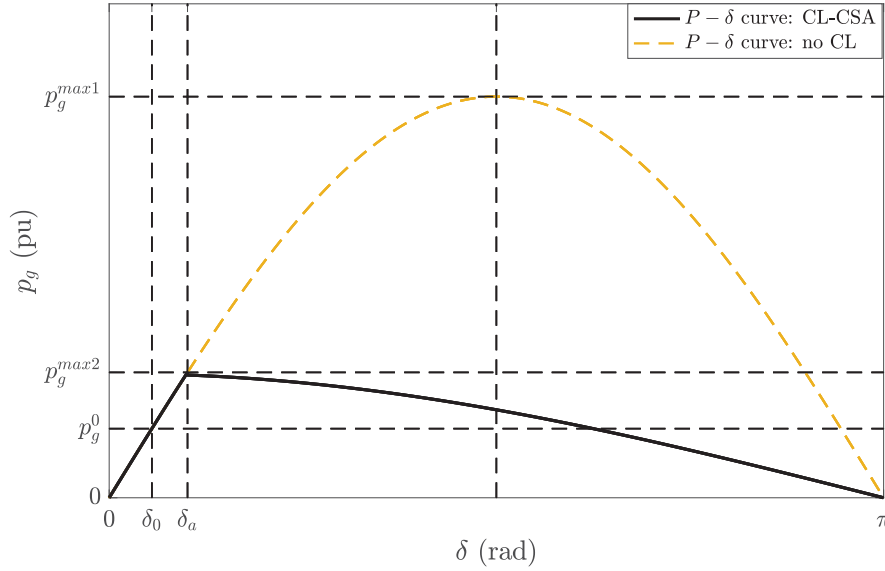
Fig. 8. GFM-VSC connected to an infinite grid.

Fig. 9. GFM-VSC with CL-CSA: $P - \delta$ curve.

Fig. 9 shows the $P - \delta$ curve of the GFM-VSC with current limiter CL-CSA. The $P - \delta$ curve of the GFM-VSC without current limiter is also represented (dashed line in yellow), for comparison purposes. In the initial operating point: $\delta = \delta_0$ and $p_g = p_g^0$. Angle δ_{cl} is defined as the angle when the fault is cleared. Without CL, the $P - \delta$ curve of the GFM-VSC is a sinusoidal curve, given by (7), where the maximum active-power injection is $p_g^{max1} = e_m^0 v_e / x_{tot}$. When the GFM-VSC has CL-CSA, the are of the $P - \delta$ curve is reduced dramatically and the maximum active-power injection of the GFM-VSC is given by $p_g^{max2} = e_m^0 v_e \sin(\delta_a) / x_{tot} < p_g^{max1}$.

The critical clearing angle δ_{cl}^{crit} is defined as the maximum angle that can take place before clearing the short circuit, without provoking loss of synchronism of the GFM-VSC. In other words, the angle when the clearing time is the CCT: $\delta_{cl}^{crit} = \delta(t = t_0 + CCT)$, where t_0 is the time when the fault has been applied. The larger is the $P - \delta$ curve, the larger will be the critical clearing angle δ_{cl}^{crit} and the larger will be the CCT. This is because, the fault can be longer, and the GFM-VSC will recover synchronism easier when the $P - \delta$ curve is larger. It is well-known that when the GFM-VSC is equipped with current limiter CL-CSA, its transient-stability margin is reduced, as can be observed in Fig. 9 (see [37] for further details).

However, the CCT depends on the $P - \delta$ curve but also depends on the particular self-synchronisation strategy used in GFM-VSC control (Fig. 3 of Section 3). Specifically, the CCT can be obtained (sometimes analytically and sometimes numerically) using the swing equation of the GFM-VSC self-synchronisation strategy and imposing the condition that the frequency of the GFM-VSC can be recovered to its pre-fault value, after the fault clearing [28]. Notice that the CCT depends also on value of the emulated inertia constant H_{GFM}. In the comparison, every GFM-VSC self-synchronisation strategy has the same value of

H_{GFM}. Therefore, conclusions related to transient-stability margin can be analysed by looking to the $P - \delta$ curve and the differential equation of the GFM-VSC strategy.

5.1. GFM-VSC self-synchronisation strategies

A qualitative analysis of GFM-VSC self-synchronisation strategies of Section 3 (see Fig. 4) is presented in this subsection. For the analysis, it is assumed that the frequency controller of GFM-VSC is slow and it has low impact on transient stability; therefore, it is neglected for simplification purposes. Naturally, in the only case that the frequency controller is considered is in the case of VSM without PLL, because it this case the damping term plays also the role of an instantaneous primary frequency response (PFR) term and it cannot be neglected. The evolution of the frequency and angle of the modulated voltage of the GFM-VSC will be analysed in a qualitative way, and the CCT of each self-synchronisation strategy will be discussed. Notice that an analytical formula of the critical clearing angle and the CCT cannot be obtained when considering the $P - \delta$ characteristic of the GFM-VSC with CL-CSA (8) and the different differential equations of the self-synchronisation strategies (swing equations). However, useful insight can be obtained by means of qualitative analysis and numerical simulation.

5.2. Strategy 1: VSM-noPLL

In the VSM without PLL scheme (Fig. 4-(a)), when a fault occurs, the active-power injection of the GFM-VSC goes to zero and the differential equation (swing equation) of this self-synchronisation strategy reads:

$$2H_{GFM} \frac{d\omega}{dt} + D_{GFM}(\omega - \omega_{0,pu}) = p_g^0 - \cancelto{0}{p_g} \tag{9}$$

Therefore, the derivative of the frequency of the GFM-VSC during the fault is given by:

$$\frac{d\omega}{dt} = \frac{1}{2H_{GFM}}[p_g^0 - D_{GFM}(\omega - \omega_{0,pu})] \tag{10}$$

Clearly, high values of the emulated inertia constant (H_{GFM}) and the damping coefficient (D_{GFM}) prevent loss of synchronism, because they reduce acceleration of the frequency of the GFM-VSC and, therefore, the increase of the angle of the modulated voltage of the GFM-VSC (δ) is also reduced. As a consequence, high values of H_{GFM} and D_{GFM} increase the critical clearing angle (δ_{cl}^{crit}) and the CCT. However, this strategy has a limitation: since the damping coefficient D_{GFM} plays two roles at the same time: the damping term and the instantaneous primary frequency controller, typical values for primary frequency control gains should be used ($D_{GFM} = 20-25$ pu), and not higher. This aspects limits the performance of the GFM-VSC in terms of transient stability.

5.3. Strategy 2: VSM-PLL

In the VSM with PLL scheme (Fig. 4-(b)), when a fault occurs, the swing equation of the GFM-VSC is given by:

$$2H_{GFM}\frac{d\omega}{dt} + D_{GFM}(\omega - \tilde{\omega}_{g,PLL}) = p_g^0 - \cancel{p_g^0} \tag{11}$$

Assuming that the grid is strong (x_g low), the estimated frequency at the connection point by the PLL is similar to the nominal frequency: $\tilde{\omega}_{g,PLL} \approx \omega_{0,pu}$. Therefore, the behaviour of the VSM-PLL strategy is the same as that of the VSM scheme without PLL (given by Eqs. (9) and (10)). However, there is an important difference, in the VSM-PLL scheme, the damping term (with damping coefficient D_{GFM}) is decoupled from the primary frequency controller. Hence, the damping coefficient could be much higher (e.g., $D_{GFM} = 100 - 300$ pu). This prevents loss of synchronism, since, during the fault, the increase of the frequency and the angle of the GFM-VSC is much lower than then one obtained with the VSM-noPLL strategy. Thus, the CCT achieved with the VSM-PLL strategy is expected to be higher than then one obtained with the VSM-noPLL strategy.

5.4. Strategy 3: VSM-Washout

In the VSM without PLL + wash-out filter scheme (Fig. 4-(c)), the damping term and the frequency controller are also decoupled. Hence, a high value of the damping coefficient can be used ($D_{GFM} = 100 - 300$ pu). For the analysis, the wash-out filter is neglected: $sT_{WD}/(1 + sT_{WD}) \approx 1$. Therefore, the CCT obtained when using strategy VSM-Washout is expected to be very similar to the one obtained when using strategy VSM-PLL. This is only true if the wash-out filter time constant (T_{WD}) is high enough.

5.5. Strategy 4: IP control

In the IP control scheme (Fig. 4-(d)), when a fault occurs, the swing equation of the GFM-VSC (in the Laplace domain) is given by:

$$\frac{1}{2sH_{GFM}}(p_g^0 - \cancel{p_g^0} - K_P\cancel{p_g^0}) = \omega \tag{12}$$

Hence,

$$\frac{d\omega}{dt} = \frac{1}{2H_{GFM}}p_g^0 \tag{13}$$

This means that the frequency increase during the fault when using IP control is higher than the one obtained in VSM with PLL. This is not trivial, since the behaviour of strategies VSM-PLL and IP control are equivalent under small disturbances, if they are properly tuned (see Section 3.5). Nevertheless, transient-stability behaviour is different when using IP control and the reason is that during the fault the active-power injection of the (p_g) goes to zero and this produces a higher acceleration of the frequency, according to the block diagram of this control strategy (Fig. 4-(d)). Therefore, the CCT obtained with IP control is expected to be lower than the one obtained with strategy VSM with PLL.

5.5.1. Conclusion

According to the theoretical analysis, the highest CCTs are achieved with strategies VSM-PLL and VSM-Washout. The CCT obtained with the strategy of VSM without PLL is expected to be lower, due to the fact that it has a lower value of the damping coefficient ($D_{GFM} = 20 - 25$ pu), because the damping term also plays the role of primary frequency controller. The CCT with IP control is expected to the lower than the one obtained with strategies VSM-PLL and VSM-Washout, because during the fault the active-power injection of the (p_g) goes to zero and this produces a higher acceleration of the frequency in the former, due to its block diagram. Qualitative analysis cannot provide conclusions about which CCT is higher: with VSM-noPLL or with IP control. If the IP control is tuned to have a high damping ratio, it is expected to have a better performance than when using strategy VSM without PLL, due to the behaviour of the GFM-VSC after the fault clearing. However, which of these two strategies will have higher CCTs would depend on the control tuning and scenarios considered.

5.6. Virtual active-power control (VAPC)

When using VAPC (Fig. 6 of Section 4.1), the unsaturated virtual active power, p_g^{virt}, is used as feedback signal in the GFM-VSC self-synchronisation strategy. This means that transient stability behaviour of the GFM-VSC is driven by $P - \delta$ curves using p_g^{virt}, independently that current limit is reached [37], which is precisely the advantage of VAPC. The unsaturated virtual active-power injection of the GFM-VSC, as a function of the angle of its modulated voltage is given by [37,38]:

$$p_g^{virt} = \begin{cases} \frac{e_m^0 v_e}{x_c + x_g} \sin\delta, & \text{if} \quad \delta < \delta_a \ (i_g < i_g^{\max}) \\ \frac{e_m^0 v_e}{x_c + x_g/K_{CL}} \sin\delta, & \text{if} \quad \delta \geq \delta_a \ (i_g = i_g^{\max}) \end{cases} \tag{14}$$

where δ_a is the angle when the current injection of the GFM-VSC reaches its current limit ($i_g = i_g^{\max}$), and the term K_{CL} is defined as:

$$K_{CL} = K_{CL}(\delta) = \frac{\bar{i}_g^{ref'}}{\bar{i}_g^{ref}} \tag{15}$$

where $\bar{i}_g^{ref'} = i_{g,d}^{ref'} + ji_{g,q}^{ref'}$ is the unsaturated current reference (before current limitation) and $\bar{i}_g^{ref} = i_{g,d}^{ref} + ji_{g,q}^{ref}$ is the saturated current reference (after current limitation) (see Fig. 2 of Section 2). Since the GFM-VSC has a CL-CSA current limiter with equal priority to d- and q-axis current injections, $\bar{i}_g^{ref'}$ and $\bar{i}_g^{ref}$ have the same phase; therefore, K_{CL} is a real number. Notice also that $K_{CL} \geq 1$ always.

Fig. 10 shows the $P - \delta$ curve of the unsaturated virtual active-power injection of the GFM-VSC (p_g^{virt}), when using VAPC and current limiter CL-CSA [37,38]. It is clear from Fig. 10 that with VAPC the $P - \delta$ curve is larger than the ones obtained with GFM-VSC without CL and with CL-CSA. Therefore, the CCT obtained with VAPC will be much higher that the ones obtained without VAPC (without CL and with CL-CSA). This is because when the current injection of the GFM-VSC reaches its current limit, the denominator of the sinusoidal expression of p_g^{virt} (14) has a lower reactance: $x_c + x_g/K_{CL}$ with $K_{CL} \geq 1$, as explained in [37,38].

As a conclusion, with VAPC the CCT of the fault can be increased significantly and VAPC can be applied to all GFM-VSC self-synchronisation strategies of Section 3.

5.7. Proposed frequency limiter

The frequency limiter for GFM-VSCs proposed in Section 4.2 is analysed now, using the $P - \delta$ curves of Fig. 9. The critical clearing angle (δ_{cl}^{crit}) is independent of the GFM-VSC self-synchronisation strategy used and it depends only on the $P - \delta$ curve. However, the proposed frequency limiter will have an impact on the behaviour of the GFM-VSC self-synchronisation strategy and, therefore, on the CCT of the fault.
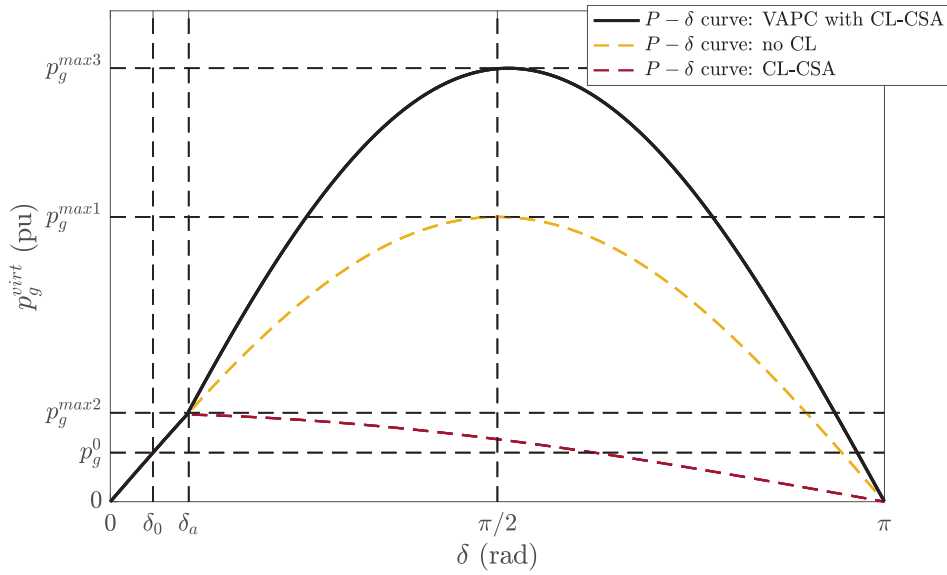
Fig. 10. GFM-VSC with Virtual active power control (VAPC) and CL-CSA: $P - \delta$ curve.

With then proposed frequency limiter, the derivative of the frequency imposed by the GFM-VSC will be given by:

$$\frac{d\omega}{dt} \begin{cases} = \text{GFM-VSC self-sync. strategy,} & \text{if} \quad \omega^{min} < \omega < \omega^{max}. \\ \geq 0, & \text{if} \quad \omega = \omega^{min}. \\ \leq 0, & \text{if} \quad \omega = \omega^{max}. \end{cases} \quad (16)$$

It is clear that if the frequency is limited, the critical clearing angle will be reached later (δ_{cl}^{crit}) and, therefore, the CCT of the fault will increase significantly. Furthermore, the proposed frequency limiter can be applied to all GFM-VSC self-synchronisation strategies of Section 3.

6. Case study and results

A 100 MVA GFM-VSC-based generator connected to an infinite grid is considered, as shown in Fig. 11. Data of the system can be found in Appendix. Simulations were carried out with VSC_Lib tool, an open-source tool based on Matlab + Simulink + SimPowerSystems developed by L2EP-LILLE in Migrate project [57–59].

Transient-stability performance of the following GFM-VSC self-synchronisation strategies of Fig. 4 will be analysed and compared:

- Strategy 1: VSM-noPLL ($D_{GFM} = 20$ pu).
- Strategy 1: VSM-noPLL ($D_{GFM} = 203$ pu) (for illustrative purposes).
- Strategy 2: VSM-PLL ($D_{GFM} = 203$ pu).
- Strategy 3: VSM-Washout ($D_{GFM} = 203$ pu, $T_{WD} = 2$ s).
- Strategy 4: IP control ($K_p = 0.0096$ pu).

The design considerations and values of the parameters are depicted in Table 2. Notice that in the case of VSM without PLL, the damping

Table 2
Design and parameters of GFM-VSC self-synchronisation strategies.

Strategy	Specified values	Calculated values
Strategy 1: VSM-noPLL	$H_{GFM} = 5$ s, $D_{GFM} = 20$ pu PFR (implicit): $K_{PFR} = D_{GFM} = 20$ pu $T_{PFR} = 0$ s	$\zeta = 0.0691$ $\omega_n = 14.47$ rad/s
Strategy 2: VSM-PLL	$H_{GFM} = 5$ s, $\zeta = 0.7$ PFR: $K_{PFR} = 20$ pu, $T_{PFR} = 1$ s	$D_{GFM} = 203$ pu $\omega_n = 14.47$ rad/s
Strategy 3: VSM-Washout	$H_{GFM} = 5$ s, $\zeta = 0.7$ PFR: $K_{PFR} = 20$ pu, $T_{PFR} = 1$ s Wash-out: $T_{WD} = 2$ s	$D_{GFM} = 203$ pu $\omega_n = 14.47$ rad/s
Strategy 4: IP control	$H_{GFM} = 5$ s, $\zeta = 0.7$ PFR: $K_{PFR} = 20$ pu, $T_{PFR} = 1$ s	$K_P = 0.0096$ pu $\omega_n = 14.47$ rad/s

coefficient plays also the role of frequency droop and a suitable proportional gain for this purpose must be used: $D_{GFM} = 20$ pu, which results in a low damping ratio. An additional case of VSM without PLL is considered using the same design criteria than the other two VSM-type strategies, but it is just for comparison purposes (VSM-noPLL with $D_{GFM} = 203$ pu).

In Section 6.1, non-linear time-domain simulations are carried out to analyse the performance of the GFM-VSC self-synchronisation strategies when a fault occurs. Section 6.2 compares the critical clearing times obtained with each GFM-VSC self-synchronisation strategy. Section 6.3 analyses the performance of VAPC and the proposed FLC, when they are applied to the different GFM-VSC self-synchronisation strategies. Finally, Section 6.4 analyses the impact on transient stability of the wash-out-filter time constant in Strategy 3 (VSM-Washout).
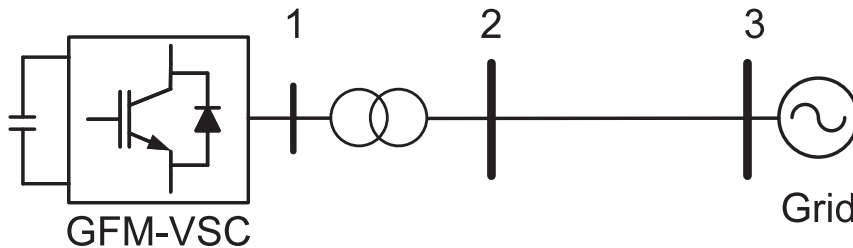

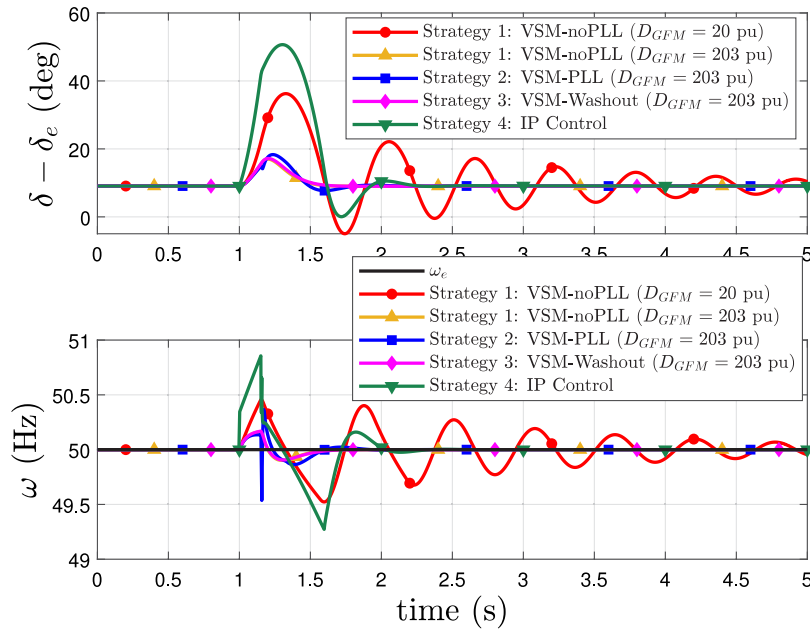**Fig. 11.** GFM-VSC connected to an infinite bus.

Fig. 12. Fault 1 cleared after 150 ms. (top) Angle difference and (bottom) Frequency of the GFM-VSC.

6.1. Short-circuit simulation

A three-phase-to-ground short circuit is applied to the line 2-3 of the test system of Fig. 11 at $t = 1$ s, close to bus 2, and it is cleared 150 ms later (Fault 1, for short). Fig. 12 shows the angle difference between the GFM-VSC and the grid ($\delta - \delta_e$) as well as the frequency deviation of the VSC with respect to the grid frequency. Synchronism is maintained in all cases, although the IP controller showed the largest angle and frequency increase during the transient. After the fault clearing, the VSM-noPLL using $D_{GFM} = 20$ pu exhibits oscillations before reaching the steady state due to its low damping factor value. However, VSM-PLL and VSM-Washout (and VSM-noPLL, but with $D_{GFM} = 203$ pu) present the smallest variation of the angle difference and the frequency of the GFM-VSC during the transient, producing the best results in terms of transient stability.

Fig. 13 displays the GFM-VSC's active and reactive power injections, and Fig. 14 shows the voltages and the current injections of the VSC. During the fault, in all self-synchronisation strategies the active power injection experiences a sharp drop, triggering the converter current limiter (see Fig. 14) and accelerating the converter. Once the fault is cleared, the active power injection sharply rises to the limit set by the current limiter ($i_s^{max} = 1.25$ pu). Finally, the GFM-VSC controls its modulated voltage according to Fig. 2, and its reactive-power injection changes accordingly.

A question that arises is, if the behaviour of VSM with PLL and the IP controller is theoretically equivalent (under small disturbances), why do they exhibit so different behaviour under large disturbances, such as short circuits. In all strategies, during the fault, the converter output power goes to zero ($p_g = 0$). In the IP controller, this leads to the acceleration of the GFM-VSC as according to Eq. (13) (see Fig. 4-(c)). Hence, the frequency change of the GFM-VSC during the fault is higher, being closer to loss of synchronism.

Finally, Fig. 15 shows the angle difference between the GFM-VSC and the grid when the clearing time of Fault 1 is 300 ms. Synchronism is lost when the GFM-VSC uses VSM-noPLL (with $D_{GFM} = 20$ pu) and IP control, while the system is stable when the GFM-VSC uses VSM-noPLL (with $D_{GFM} = 203$ pu), with VSM-PLL and with VSM-Washout, confirming the conclusions drawn previously.

Table 3
Critical clearing times (CCTs).

GFM-VSC control strategy	CCT (ms)
Strategy 1: VSM-noPLL ($D_{GFM} = 20$ pu)	280
Strategy 1: VSM-noPLL ($D_{GFM} = 203$ pu)	1600
Strategy 2: VSM-PLL ($D_{GFM} = 203$ pu)	1700
Strategy 3: VSM-Washout ($D_{GFM} = 203$ pu)	1020
Strategy 4: IP control	190

6.2. Critical clearing times

The Critical Clearing Time (CCT) of a fault is defined as the maximum duration that it can have without provoking loss of synchronism, and it is normally used as an indicator for transient-stability margin. Table 3 presents the critical clearing times (CCTs), in milliseconds (ms), of the fault simulated in previous subsection (Fault 1, applied to line 2-3, close to bus 2, of the system of Fig. 11) obtained for the different GFM-VSC self-synchronisation strategies. The CCT evaluation takes into account the presence or absence of two additional mechanisms: the proposed frequency limiter (FLC) and the virtual active power control (VAPC).

Strategy 1 (VSM-noPLL) was evaluated with two different values of the damping parameter ($D_{GFM} = 20$ and $D_{GFM} = 203$ pu).

Strategies VSM-noPLL with $D_{GFM} = 203$ pu, and VSM-PLL using the same damping coefficient, exhibit the largest CCTs (1600 ms and 1700 ms, respectively), while VSM-noPLL but with $D_{GFM} = 20$ pu has a smaller CCT (280 ms), indicating a poorer transient-stability performance. Furthermore, the IP-control strategy has the lowest CCT (190 ms), meaning the worst transient-stability margin. Although the IP controller is similar to the VSM-PLL strategy in small signal analysis, it differs under large disturbances, due to the fact that the active-power injection goes close to zero during the fault. This occurs at the frequency change of the GFM-VSC is higher than the one obtained with other self-synchronisation strategies, as discussed in previous subsection.

6.3. Performance of virtual active power control (VAPC) and proposed frequency (FLC) limiter

Fault 1 with a clearing time of 300 ms is simulated now. Fig. 16 shows the angle difference of the GFM-VSC when VAPC is implemented
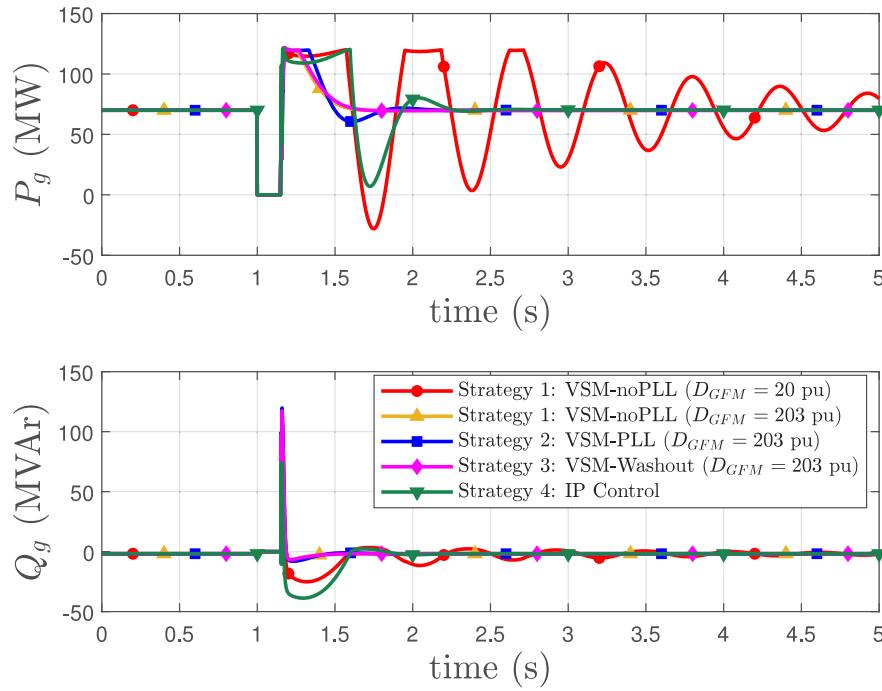
Fig. 13. Fault 1 cleared after 150 ms. (top) Active and (bottom) Reactive of the GFM-VSC.
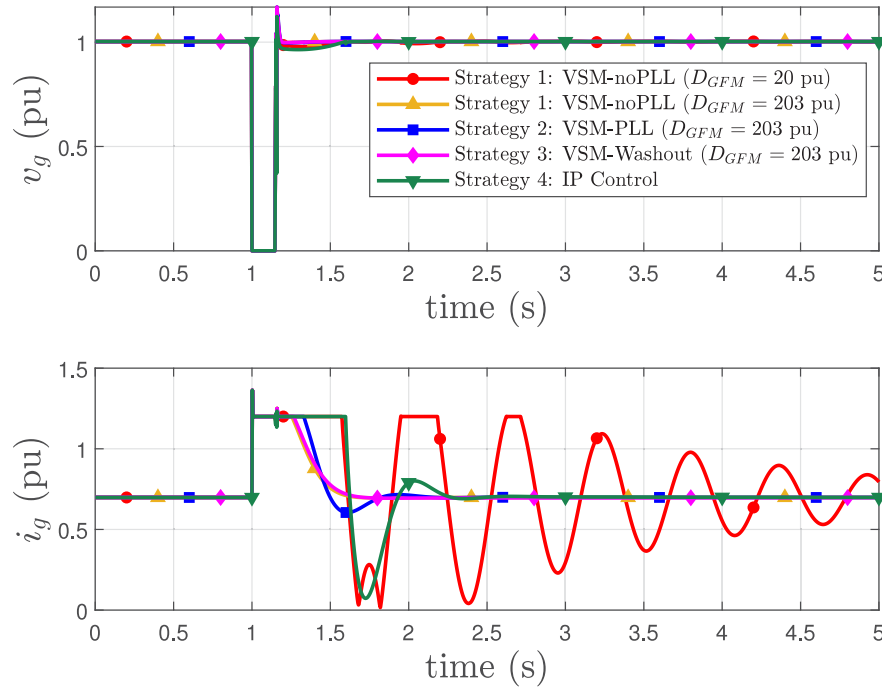

Fig. 14. Fault 1 cleared after 150 ms. (top) voltage at the terminal and (bottom) Current injection of the GFM-VSC.

(Section 4.1). VAPC concept improves transient stability when it is applied to all GFM-VSC self-synchronisation strategies, since synchronism is maintained in all cases (see Fig. 15 for comparison).

Fault 1 with a clearing time of 300 ms is simulated now. Fig. 17 shows the angle difference of the GFM-VSC when the proposed frequency limitation algorithm (FLC) is implemented (Section 4.2), also for Fault 1 with a clearing time of 300 ms. The frequency of the GFM-VSC is also showed, to understand the frequency limitation process produced by FLC. Parameters of Fig. 7 and Eq. (6) are set to $\Delta\omega_i^{max} = 0.005$ pu, $v_{A,i} = 0.5$ pu and $v_{B,i} = 0.9$. The proposed frequency limiter

(FCL) also improves transient stability when it is applied to all GFM-VSC self-synchronisation strategies, because synchronism is maintained in all cases. Notice that the frequency of the GFM-VSC is limited during the fault, preventing loss of synchronism (see Fig. 17).

Finally, Table 4 shows the CCTs of Fault 1 under different combinations of FLC and VAPC activation or deactivation:

- **No-FLC/No-VAPC** (Base case, second column in Table 4): Neither the FLC nor VAPC is used.
- **No-FLC/VAPC** (third column in Table 4): VAPC is used only.
- **FLC/No-VAPC** (fourth column in Table 4): With FLC only.
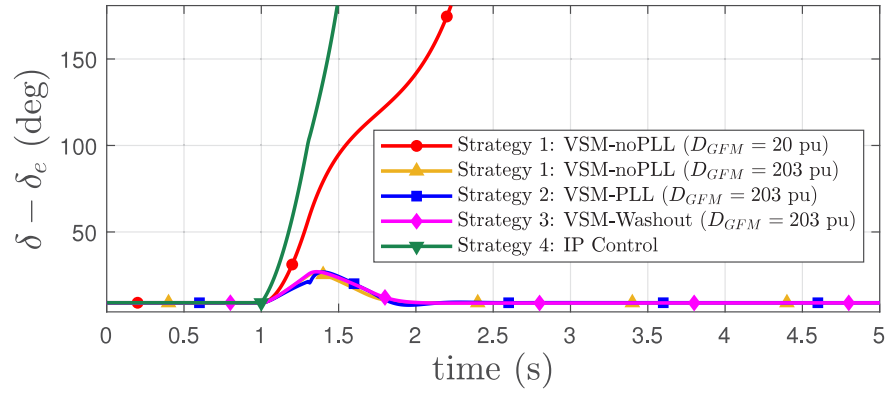
Fig. 15. Fault 1 cleared after 300 ms: Angle difference of the GFM-VSC.
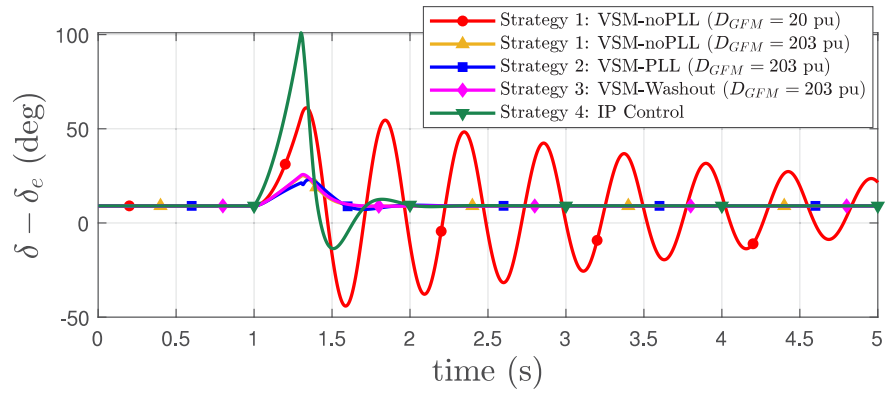

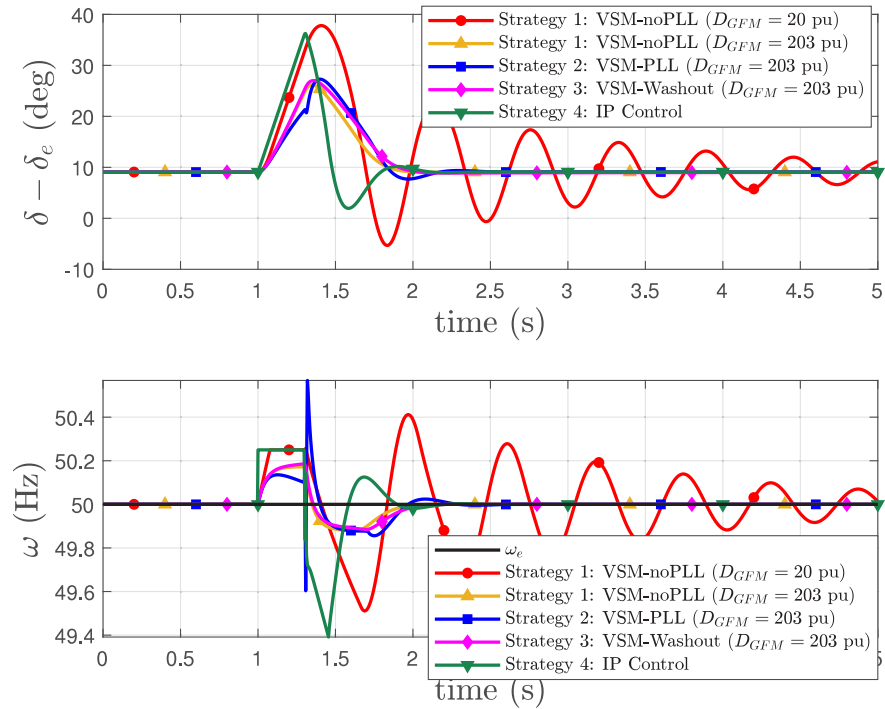**Fig. 16.** GFM-VSC with VAPC. Fault 1 cleared after 300 ms: Angle difference of the GFM-VSC.

Fig. 17. GFM-VSC with proposed FLC. Fault 1 cleared after 300 ms. (top) Angle difference and (bottom) Frequency of the GFM-VSC.

Table 4
Critical clearing times (CCTs) with and without the proposed frequency limiter (FLC) and virtual active power control (VAPC).

GFM-VSC control strategy	CCT (ms)			
	No-FLC		FLC	
	No-VAPC	VAPC	No-VAPC	VAPC
Strategy 1: VSM-noPLL (D_{GFM} = 20 pu)	280	540	940	1790
Strategy 1: VSM-noPLL (D_{GFM} = 203 pu)	1600	2640	1600	2640
Strategy 2: VSM-PLL (D_{GFM} = 203 pu)	1700	3440	1720	3830
Strategy 3: VSM-Washout (D_{GFM} = 203 pu)	1020	1900	1020	1970
Strategy 4: IP control	190	390	1160	1830

Table 5
CCTs of VSM-Washout strategy with different time constants.

GFM-VSC control strategy	CCT (ms)
Strategy 3: VSM-Washout (T_{WD} = 0.02 s)	0
Strategy 3: VSM-Washout (T_{WD} = 0.2 s)	460
Strategy 3: VSM-Washout (T_{WD} = 2 s)	1020
Strategy 3: VSM-Washout (T_{WD} = 5 s)	1290

- **FLC/VAPC** (fifth column in Table 4): Both mechanisms are activated.

The third column in Table 4 (No-FLC/VAPC) demonstrates significant improvements in the CCTs when using VAPC. Meanwhile columns 4 and 5 (FLC/No-VAPC and FLC/VAPC, respectively) show the results by applying the proposed frequency limiter for GFM-VSCs. The proposed frequency limiter also results in significant improvements in CCTs in all the GFM-VSC self-synchronisation strategies.

VSM-noPLL strategy with the lowest damping factor (D_{GFM} = 20 pu) shows a significant increase in CCT when FLC and/or VAPC are applied. VSM-noPLL experiences a notable increase in CCT from 280 ms (No-FLC/No-VAPC) to 940 ms when the frequency limiter is enabled (FLC/No-VAPC), showcasing its effectiveness in improving stability. CCTs reach 1790 ms when both FLC and VAPC are enabled (FLC/VAPC), compared to the base case.

Significant improvements have also been made to the IP-control strategy, which benefits considerably from the use of FLC and VAPC. CCT increases from 190 ms without the mechanisms to 1830 ms with both enabled.

As a conclusion, the concept of VAPC and the proposed FLC can be applied to all GFM-VSC self-synchronisation strategies analysed and they are effective to improve transient stability in all cases. Furthermore, VAPC and FLC can be used together, obtaining further improvements.

Due to non-linearities, it is not easy to find a general pattern when quantifying the improvements that can be achieved either with VAPC or with FLC methods, separately. Key aspects are the following:

- FLC method limits the frequency imposed by the GFM-VSC. Therefore, it is expected that FLC method will have a key role during the fault.
- VAPC method modifies the $P - \delta$ curve of the GFM-VSC curve, making it larger. Therefore, it is expected that VAPC method will have a significant impact after the fault clearing.

When analysing in detail each GFM-VSC self-synchronisation strategy, the following conclusions are obtained:

- Strategy 1: VSM-noPLL (D_{GFM} = 20 pu): The damping term is low ($D_{GFM}\Delta\omega$), because the damping coefficient is low (D_{GFM} = 20 pu). Hence, the frequency increases during the fault, and the frequency increase is much higher than in other cases. FLC method limits the frequency during the fault. Therefore, FLC method (CCT=940 ms) is more effective than VAPC method (CCT=540 ms).

- Strategy 1 (VSM-noPLL), Strategy 2 (VSM-PLL) and Strategy 3 (VSM-Washout), with D_{GFM} = 203 pu. The damping term is high. Hence, during the fault, the damping term limits the frequency increase. Observations indicate that the role of synchronisation process after the fault clearing (e.g., making the $P-\delta$ curve larger) is more relevant. Therefore, when using these strategies, VAPC method is more effective than FLC method.
- Strategy 4: IP Control. The damping ratio of the system in this case is also high, due to the design of the controller (see Table 2 of the paper). However, the frequency increase during the fault is high because the control structure of the controller, as discussed in Section 5.5 (see Eq. (13) or the new version of the paper). Using FLC method limits the frequency increase during the fault. Therefore, FLC method (CCT=1160 ms) is more effective than VAPC method (CCT=390 ms).

Finally, it is worth to highlight that the paper analysed solid three-phase-to-ground short circuits, which cause a 100% voltage sag. These types of faults are often used to assess transient stability, because solid three-phase-to-ground short circuits are the most critical case. However, the conclusions obtained in the paper are still valid when faults with higher impedance occur. Naturally, the numbers will change (in fact all the CCTs will increase if the impedance of the fault increase), but the conclusions are still valid.

6.4. Strategy 3: VSM-Washout - Effect of the wash-out filter time constant

In Strategy 3 (VSM-Washout), the time constant of the wash-out filter (T_{WD}) has an impact of the performance of Strategy 3 (VSM-Washout) and it is analysed now. A summary of the guidelines for the design of the wash-out filter time constant is as follows (Section 3.5):

- Parameter T_{WD} should be relatively high, in order to avoid interactions and achieve a good performance in terms of small-signal stability and transient stability. Ref. [52] proposes a curve for feasible regions of parameters D_{GFM} and T_{WD} (see Fig. 4-(c)), in terms of transient stability, concluding that $T_{WD} \geq 1$ s could be a reasonable value for typical parameters.
- Parameter T_{WD} should not be excessively high, to avoid active-power changes during very-slow fluctuations.
- Then, the guidelines for the design of the GFM-VSC self-synchronisation strategies can be used (Table 1 of Section 3.5), assuming a fixed value of T_{WD}. Finally, the behaviour should be checked also by time-domain simulation.

Taking the aspects above into account, the choice of the wash-out filter time constant for Strategy 3 used in this work was T_{WD} = 2 s.

The impact of the wash-out filter in Strategy 3 is analysed now for different values of T_{WD}: T_{WD} = 20 ms, T_{WD} = 200 ms, T_{WD} = 2 s and T_{WD} = 5 s. Fig. 18 shows the angle difference of the GFM-VSC and the infinite grid, when Fault 1 with a clearing time of 300 ms is simulated. When T_{WD} = 20 ms, synchronism is lost. When T_{WD} = 200 ms, synchronism is maintained, but the angle excursions are high. For T_{WD} = 2 s and T_{WD} = 5 s, synchronism is maintained and angle excursions are much lower than in the other cases.

In strategy 3 (VSM-Washout), transient-stability behaviour should be also taken into account. In previous work, the design of the wash-out filter time constant in strategy VSM-Washout has not been addressed explicitly. However, Ref. [52] has analysed the impact of the wash-out filter in the so-called transient damping method (TDM), and conclusions can be applied directly to the VSM-Washout strategy. The work in [52] proposes a curve for feasible regions of parameters D_{GFM} and T_{WD}, in terms of transient stability. Mainly, in order to use high values of D_{GFM}, the wash-out filter time constant should be high enough, concluding that $T_{WD} \geq 1$ s could be a reasonable value, for the test system analysed. In addition, in Strategy 3 the wash-out filter add a state variable and the closed-loop system dynamics is more
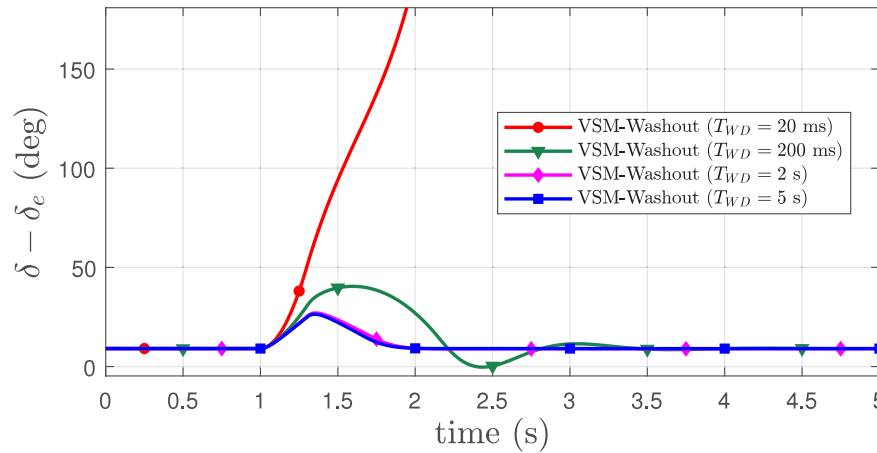
Fig. 18. Fault 1 cleared after 300 ms: Angle difference of the GFM-VSC.

complex and it is not a second-order system any more. However, this aspect can be addressed by using a high enough value of T_{WD} and it is recommended to check the results of the design by time-domain simulation. Finally, notice that the wash-out filter time constant T_{WD} should not be excessively high, because it would not be able to avoid active-power changes under frequency offsets, which is its role.

Finally, Table 5 depicts the CCTs of fault 1 when Strategy 3 is used, for the different values of the washout filter time constant. The highest CCTs are obtained with $T_{WD} = 2$ s and $T_{WD} = 5$ s, proving clearly that the best results are obtained with these values. When $T_{WD} = 20$ ms, the system is unstable even for small perturbations, that is why the CCT is 0 ms. This proves that too low values of T_{WD} will produce poor results.

7. Conclusions

This paper analysed and compared transient-stability performance of various self-synchronisation strategies for GFM-VSCs: VSM-noPLL, VSM-PLL, VSM-Washout and IP control. The paper also analysed different methods to be applied to GFM-VSC self-synchronisation strategies, aimed to improve their transient-stability performance: the concept of virtual unsaturated active-power controller (VAPC), proposed in previous work, and an algorithm for frequency limitation in the GFM-VSCs (FLC), which was proposed in this paper. The conclusions obtained in this paper can be summarised as follows:

- The four self-synchronisation mechanisms for GFM-VSCs analysed in this work (VSM-noPLL, VSM-PLL, VSM-Washout and IP control) can have a similar behaviour under small disturbances by proper tuning of the parameters. However, they can have different behaviour under large disturbances (transient stability), due to non-linearities.
- Strategies VSM-PLL and VSM-Washout produce the best results in terms of transient stability.
- Strategies VSM-noPLL and IP control produce the lowest critical clearing times (CCTs).
- Strategy VSM-noPLL ($D_{GFM} = 20$ pu) produces worse results than other strategies in terms on transient stability not due to its control structure, but due to the design of the parameters. Since the damping coefficient used in the self-synchronisation strategy plays also the role of primary frequency controller, it should be designed with typical values for primary-frequency controller proportional gains, which produces a dynamic response of the GFM-VSC with lower damping ratio than with other options, and this jeopardises transient stability.
- The IP control produces worse results than other options in therms of transient stability due to the active-power signal which is subtracted after the inertial-response term. When a fault occurs,

the voltage at the PCC becomes close to zero; therefore, the active-power injection becomes close to zero too, producing a high variation of the frequency of the GFM-VSC during the fault, being more vulnerable to loss of synchronism.
- The concept of VAPC (proposed in previous work) can be applied to all GFM-VSC self-synchronisation strategies and it improves transient stability in all cases.
- The proposed algorithm for frequency limitation (FLC) can be applied to all GFM-VSC self-synchronisation strategies and it improves transient stability in all cases.
- Applying Virtual Active Power Control (VAPC) or the proposed Frequency Limitation Control (FLC) together significantly improves transient stability of the four GFM-VSC self-synchronisation strategies analysed, increasing the CCTs.
- In VSM-Washout strategy, the wash-out-filter time constant should be high enough to produce good results in terms of transient stability. Reasonable values could be in the range $T_{WD} = 1 - 10$ s, for the test system considered in this paper.

Finally, some proposals for future work are discussed. In this work, GFM-VSCs are represented in the AC side and their primary energy source or energy storage has not been modelled. Transient stability improvements related to GFM-VSC self-synchronisation strategies will cause changes on the DC voltage. Therefore, an interesting research line for future work is the analysis of GFM-VSC power converters with detailed representation of primary energy source or energy storage, for different applications.

CRediT authorship contribution statement

Régulo E. Ávila-Martínez: Writing – review & editing, Writing – original draft, Visualization, Validation, Software, Resources, Project administration, Methodology, Investigation, Formal analysis, Data curation, Conceptualization. **Xavier Guillaud:** Writing – review & editing, Supervision, Investigation, Conceptualization. **Javier Renedo:** Writing – review & editing, Writing – original draft, Supervision, Methodology, Investigation, Formal analysis, Conceptualization. **Luis Rouco:** Writing – review & editing, Supervision, Investigation, Funding acquisition, Formal analysis, Conceptualization, Project administration. **Aurelio Garcia-Cerrada:** Writing – review & editing, Validation, Supervision, Methodology, Funding acquisition, Formal analysis, Conceptualization, Project administration. **Lukas Sigrist:** Writing – review & editing, Visualization, Supervision, Investigation, Formal analysis, Conceptualization.

Table 6
Parameters of the GFM-VSCs.

Parameters VSC's rating are base values for pu	Values
Rating VSC, DC voltage, AC voltage	100 MVA, 640 kV, 400 kV
Max. current	1.20 pu (equal priority for $d-q$ axes)
Series resistance (r_c)/reactance (x_c)	0.005 pu/0.15 pu
(series reactor + transformer)	
(transformer: 100 MVA 400/320 kV)	
Current control bandwidth ($\omega_{n,CC}$)	1500 rad/s
Current control prop./int. gains ($K_{C,P}/K_{C,I}$)	1.0027 pu/1074.3 pu/s
Quasi-static model, virt. reactance (x_v/x_{ev})	0 pu/0.15 pu
Emulated inertia (H_{GFM})	5 s
Primary freq. controller ($K_{PFR,i}/T_{PFR}$)	20 pu/1 s
Primary freq. controller limit (Δp_g^{max})	1 pu
PLL control bandwidth ($\omega_{n,PLL}$)	500 rad/s
PLL control porp./int. gains ($K_{P,PLL}/K_{I,PLL}$)	3.1831 pu/795.7747 pu/s
PLL frequency saturation ($\Delta\omega_{PLL}^{max}$)	± 0.1 pu

Declaration of competing interest

The authors declare that they have no known competing financial interests or personal relationships that could have appeared to influence the work reported in this paper.

Appendix. Data

Data of GFM-VSCs are provided in Table 6. Nominal voltage and frequency of the system are 220 kV and 50 Hz, respectively. Parameters of line 2-3 are $r_g = 0.01$ pu, $x_g = 0.1$ pu (base values for pu: 220 kV and 100 MVA). Initial operating point of the GFM-VSC is $P_g^0 = 70$ MW and $v_g^0 = 1$ pu. Constant modulated voltage set-point term was set to $e_m^0 = 1.0057$ pu.

When using the frequency limiter (FCL) proposed in Section 4.2, parameters of Fig. 7 and (6) are set to $\Delta\omega^{max} = 0.005$ pu, $v_A = 0.5$ pu and $v_B = 0.9$ pu.

Data availability

No data was used for the research described in the article.

References

[1] Paolone M, Gaunt T, Guillaud X, Liserre M, Meliopoulos S, Monti A, Van Cutsen T, Vittal V, Vournas C. Fundamentals of power systems modelling in the presence of converter-interfaced generation. Electr Power Syst Res 2020;189(106811):1–33.

[2] Strunz K, Almunem K, Wulkow C, Kuschke M, Valescudero M, Guillaud X. Enabling 100% renewable power systems through power electronic grid-forming converter and control: System integration for security, stability, and application to europe. In: Proceedings of the IEEE, vol. 111, (7):2023, p. 891–915.

[3] Cardozo C, Prevost T, Huang S-H, Lu J, Modi N, Hishida M, Li X, Abdalrahman A, Samuelsson P, Van Cutsem T, Laba Y, Lamrani Y, Colas F, Guillaud X. Promises and challenges of grid forming: Transmission system operator, manufacturer and academic view points. Electr Power Syst Res 2024;235:1–35, 110855.

[4] Barker C, Adamczyk A, Fradley J, Jasim O. Providing Synchronous Grid Forming Capability through HVDC transmission. In: The 17th international conference on AC and DC power transmission (ACDC 2021), vol. 2021, 2021, p. 161–6.

[5] Zhang L, Harnefors L, Nee H-P. Power-Synchronization Control of Grid-Connected Voltage-Source Converters. IEEE Trans Power Syst 2010;25(2):809–20.

[6] Zhong Q-C, Weiss G. Synchronverters: Inverters that mimic synchronous generators. IEEE Trans Ind Electron 2011;58(4):1259–67.

[7] D'Arco S, Suul JA. Equivalence of virtual synchronous machines and frequency-droops for converter-based microgrids. IEEE Trans Smart Grid 2014;5(1):394–5.

[8] D'Arco S, Suul JA, Fosso OB. A Virtual Synchronous Machine implementation for distributed control of power converters in SmartGrids. Electr Power Syst Res 2015;122:180–97.

[9] Roldán-Pérez J, Rodríguez-Cabero A, Prodanovic M. Design and analysis of virtual synchronous machines in inductive and resistive weak grids. IEEE Trans Energy Convers 2019;34(2):1818–28.

[10] Rocabert J, Luna A, Blaabjerg F, Rodríguez P. Control of power converters in AC microgrids. IEEE Trans Power Electron 2012;27(11):4734–49.

[11] Qoria T, Rokrok E, Bruyere A, Francois B, Guillaud X. A PLL-Free grid-forming control with decoupled functionalities for high-power transmission system applications. IEEE Access 2020;106765:197 363–78.

[12] Rodriguez Amenedo JL, Gomez SA, Alonso-Martinez J, De Armas MG. Grid-Forming Converters Control Based on the Reactive Power Synchronization Method for Renewable Power Plants. IEEE Access 2021;9:67 989–8 007, rodriguezA.

[13] Azizi Aghdam S, Agamy M. Virtual oscillator-based methods for grid-forming inverter control: A review. IET Renew Power Gener 2022;16:835–55.

[14] Groß D, Colombino M, Brouillon J-S, Dörfler F. The Effect of Transmission-Line Dynamics on Grid-Forming Dispatchable Virtual Oscillator Control. IEEE Trans Control Netw Syst 2019;6(3):1148–60.

[15] Arghir C, Jouini T, Dörfler F. Grid-forming control for power converters based on matching of synchronous machines. Automatica 2018;95:273–82.

[16] Mandrile F, Mallemaci V, Carpaneto E, Bojoi R. Lead–lag filter-based damping of virtual synchronous machines. IEEE Trans Ind Appl 2023;59(6):6900–13.

[17] Klaes NR, Fortmann J. Immunity of grid-forming control without energy storage to transient changes of grid frequency and phase. IEEE Open J Ind Electron Soc 2025;6:265–76.

[18] Girona-Badia J, Albernaz Lacerda V, Westerman Spier D, Prieto-Araujo E, Gomis-Bellmunt O. Resource-aware grid-forming synchronization control: Design, analysis and validation. IEEE Trans Energy Convers 2025;40(3):2548–61.

[19] Puricelli FG. Bipolar vsc-hvdc links with grid-forming converters – dynamic performance and small-signal stability assessment. In: Institute of electrical power systems. [Ph.D. thesis], KU Leuven, Belgium; 2025.

[20] Puricelli FG, Rault P, Cardozo C, Beerten J. Analysis and damping of grid-forming converters interactions in bipolar hvdc connections using a coordinate transformation approach. Int J Electr Power Energy Syst 2025;165(110469):1–11.

[21] Mo O, D'Arco S, Suul JA. Evaluation of Virtual Synchronous Machines With Dynamic or Quasi-Stationary Machine models. IEEE Trans Ind Electron 2017;64(7):5952–62.

[22] Girona-Badia J, Olives-Camps JC, Albernaz Lacerda V, Prieto-Araujo E, Gomis-Bellmunt O. Control performance and stability analysis of frequency estimator in grid-forming synchronization control. J Mod Power Syst Clean Energy 2025;1–12. http://dx.doi.org/10.35833/MPCE.2025.000144.

[23] Hatziargyriou N, Milanović JV, Rahmann C, Ajjarapu V, Canizares C, Erlich I, Hill D, Hiskens I, Kamwa I, Pal B, Pourbeik P, Sanchez-Gasca JJ, Stanković A, Van Cutsem T, Vittal V, Vournas C. Definition and classification of power system stability - revisited and extended. IEEE Trans Power Syst 2021;36(4):3271–81.

[24] Andrade F, Cusidó J, Romeral L. Transient stability analysis of inverter-interfaced distributed generators in a microgrid system. In: Proc European conference on power electronics and applications, birmingham. UK; 2011, p. 1–10.

[25] Shuai Z, Shen C, Liu X, Li Z, Shen ZJ. Transient angle stability of virtual synchronous generators using lyapunov's direct method. IEEE Trans Smart Grid 2018;10(4):4648–61.

[26] Cheng H, Shuai Z, Shen C, Liu X, Li Z, Shen ZJ. Transient angle stability of paralleled synchronous and virtual synchronous generators in islanded microgrids. IEEE Trans Power Electron 2020;35(8):1019–33.

[27] Pan D, Wang X, Liu F, Shi R. Transient stability of voltage-source converters with grid-forming control: A design-oriented study. IEEE J Emerg Sel Top Power Electron 2020;8(2):1019–33.

[28] Qoria T, Gruson F, Colas F, Denis G, Prevost T, Guillaud X. Critical clearing time determination and enhancement of grid-forming converters embedding virtual impedance as current limitation algorithm. IEEE J Emerg Sel Top Power Electron 2020;8(2):1050–61.

[29] Ledesma P, Arredondo F, Moreno MA. Contribution of grid-forming control to angle stability in the iberian peninsula. IET Gener Transm Distrib 2025;1–10. http://dx.doi.org/10.1049/gtd2.70076.

[30] Qoria T, Gruson F, Colas F, Kestelyn X, Guillaud X. Current limiting algorithms and transient stability analysis of grid-forming VSCs. Electr Power Syst Res 2020;189(106726):1–8.

[31] Choopani M, Hosseinian SH, Vahidi B. New transient stability and LVRT improvement of multi-VSG grids using the frequency of the center of inertia. IEEE Trans Power Syst 2020;35(1):527–38.

[32] Chen M, Zhou D, Blaabjerg F. Enhanced Transient Angle Stability Control of Grid-Forming Converter Based on Virtual Synchronous Generator. IEEE Trans Ind Electron 2022;69(9):9133–44.

[33] Xiong X, Wu C, Blaabjerg F. An Improved Synchronization Stability Method of Virtual Synchronous Generators Based on Frequency Feedforward on Reactive Power Control loop. IEEE Trans Power Electron 2021;36(8):9136–48, [Online]. Available: https://ieeexplore.ieee.org/document/9328607/.

[34] Ávila Martínez RE, Renedo J, Rouco L, García-Cerrada A, Sigrist L, Qoria T, Guillaud X. Fast Voltage Boosters to Improve Transient Stability of Power Systems With 100% of Grid-Forming VSC-Based Generation. IEEE Trans Energy Convers 2022;37(4):2777–89.

[35] Si W, Fang J. Transient Stability Improvement of Grid-Forming Converters Through Voltage Amplitude Regulation and Reactive Power injection. IEEE Trans Power Electron 2023;38(10):12 116–25, [Online]. Available: https://ieeexplore.ieee.org/document/10167833/.

[36] Luo X, Pavan Kumar Y, Kumar Singh A, Batzelis EI, Saridaki G, Kotsampopoulos P, Hatziargyriou N. In: Boundary analysis of damping methods for virtual synchronous generators, vol. 499874, 2025, p. 1–5, Pre-print, Online: https://eprints.soton.ac.uk/499874/. [Last Access 28 July 2025].

[37] Vatta Kkuni K, Yang G. Effects of current limit for grid forming converters on transient stability: Analysis and solution. Int J Electr Power Energy Syst 2024;158(109919):1–8.

[38] Laba Y, Bruyère A, Colas F, Guillaud X. Virtual Power-Based Technique for Enhancing the Large Voltage Disturbance Stability of HV Grid-Forming converters. In: 2023 25th European conference on power electronics and applications (EPE'23 ECCE europe). Aalborg, Denmark: IEEE; 2023, p. 1–8.

[39] Laba Y, Colas F, Bruyère A, Prevost T, Torresan G, Legrand X, Guillaud X. Enhancing large disturbance stability of direct voltage grid-forming converters through integration of the virtual power method. IEEE J Emerg Sel Top Power Electron 2025;1–13. http://dx.doi.org/10.1109/JESTPE.2025.3574104.

[40] Camboni A, Mallemaci V, Mandrile F, Bojoi R. The virtual power feedback: Enhancing the transient stability of virtual synchronous generators under current limitation. IEEE Open J Ind Appl 2025;1–16. http://dx.doi.org/10.1109/OJIA.2025.3586412.

[41] Collados-Rodriguez C, Westerman Spier D, Cheah-Mane M, Prieto-Araujo E, Gomis-Bellmunt O. Preventing loss of synchronism of droop-based grid-forming converters during frequency excursions. Int J Electr Power Energy Syst 2023;148:108989.

[42] Du W, Lasseter RH, Khalsa AS. Survivability of autonomous microgrid during overload events. IEEE Trans Smart Grid 2019;10(3):3515–24.

[43] Du W, Nguyen QH, Wang S, Kim J, Liu Y, Zhu S, Tuffner FK, Huang Z. Positive-sequence modeling of droop- controlled grid-forming inverters for transient stability simulation of transmission systems. IEEE Trans Power Deliv 2024;39(3):1736–48.

[44] Mohiuddin SM, Du W, Lyu X, Kim J, Nguyen QH. A two-stage current limiting control strategy for direct-droop-controlled grid-forming inverters. IEEE Trans Ind Appl 2025;61(4):6472–83.

[45] Zhao X, Flynn D. Freezing grid-forming converter virtual angular speed to enhance transient stability under current reference limiting. In: Proc. IEEE 21st workshop on control and modeling for power electronics. Aalborg, Denmark; 2020, p. 1–7.

[46] Zhao X, Flynn D. Stability enhancement strategies for a 100% grid-forming and grid-following converter-based irish power system. IET Renew Power Gener 2022;16:125–38.

[47] Dadjo Tavakoli S, Prieto-Araujo E, Gomis-Bellmunt O. Fault ride-through control based on voltage priorization for grid-forming converters. IET Renew Power Gener 2022;17:1370–84.

[48] Li Y, Lu Y, Yang J, Liu J, Mu T, Ye H, Du Z. Synchronization stability of multiple vsgs embedded power system with controller limits. IEEE Trans Power Syst 2024;1–16. http://dx.doi.org/10.1109/TPWRS.2024.3398637.

[49] Kkuni K Vatta, Mohan S, Yang G, Xu W. Comparative assessment of typical control realizations of grid forming converters based on their voltage source behaviour. Energy Rep 2023;9:6042–62.

[50] Rokrok E, Qoria T, Bruyere A, Francois B, Guillaud X. Classification and dynamic assessment of droop-based grid-forming control schemes: Application in HVDC systems. Electr Power Syst Res 2020;189(106765):1–7.

[51] DIgSILENT. Grid-forming Converter Templates. Droop Controlled Converter, Synchronverter, Virtual Synchronous machine. In: PowerFactory - dIgSILENT - technical reference. Tech. Rep., Germany; 2022.

[52] Xiong X, Wu C, Cheng P, Blaabjerg F. An optimal damping design of virtual synchronous generators for transient stability enhancement. IEEE Trans Power Electron 2021;36(10):11 026–30.

[53] Ávila Martínez RE, Renedo J, Rouco L, Garcia-Cerrada A, Sigrist L, Guillaud X, Qoria T. Impact of current limiters and fast voltage boosters in grid-forming vsc-based generators on transient stability. Electr Power Syst Res 2024;235(110753):1–11.

[54] Kundur P. Power system stability and control. New York, NY, USA: McGraw Hill Education; 1994.

[55] Gómez-Expósito A, Conejo AJ, Canizares (Coordinators) CA. Electric energy systems: analysis and operation. Boca Raton, FL, USA: CRC press, Taylor & Francis Group; 2018.

[56] Chatterjee D, Johnson B, Seo G-S. Is equal area criterion applicable for transient stability assessment of grid-forming inverters?. 2025, http://dx.doi.org/10.36227/techrxiv.174889575.57556923/v1, 1–6. TechRxiv, pre-print.

[57] L2EP-LILLE. VSC_lib: Grid forming models for Matlab/SimPowerSystem. 2020, https://github.com/l2ep-epmlab/. [Accessed 08 July 2020].

[58] Qoria T, Cossart Q, Li C, Guillaud X, Colas F, Gruson F, Kestelyn X. WP3-Control and Operation of a Grid with 100% Converter-Based Devices. Deliverable 3.2: Local control and simulation tools for large transmission systems. In: MIGRATE project. Tech. Rep., 2018.

[59] Qoria T, Gruson F, Colas F, Denis G, Prevost T, Guillaud X. Inertia effect and load sharing capability of grid forming converters connected to a transmission grid. In: 15th IET int. conf. on AC and DC power transmission (ACDC). coventry, UK; 2019, p. 1–6.